Cell Biology
Immunology and Inflammation

RAS-p110a signalling in macrophages is required for effective inflammatory response and resolution of inflammation

Reviewed Preprint
v2 • November 14, 2024
Revised by authors

Reviewed Preprint
v1 • April 12, 2024

Alejandro Rosell, Agata A Krygowska, Marta Alcón Pérez, Cristina Cuesta, Mathieu-Benoit Voisin, Juan de Paz, Héctor Sanz-Fraile, Vinothini Rajeeve, Alberto Berral-González, Ana Carreras-González, Ottilie Swinyard, Enrique Gabandé-Rodriguez, Julian Downward, Jordi Alcaraz, Juan Anguita, Carmen García-Macías, Javier De Las Rivas, Pedro Cutillas, Esther Castellano

Tumour-Stroma Signalling Lab., Centro de Investigación del Cáncer, Instituto de Biología Molecular y Celular del Cáncer, Consejo Superior de Investigaciones Científicas (CSIC)-Universidad de Salamanca, Campus Miguel de Unamuno, Salamanca, Spain • Centre for Cancer and Inflammation, Barts Cancer Institute, Queen Mary University of London, London, United Kingdom • Centre for Microvascular Research, William Harvey Research Institute, Queen Mary University of London, London, United Kingdom • Unit of Biophysics and Bioengineering, Department of Biomedicine, School of Medicine and Health Sciences, Universitat de Barcelona, Barcelona, Spain • Centre for Cancer Genomics and Computational Biology, Cell Signalling and Proteomics Laboratory, Barts Cancer Institute, Queen Mary University of London, London, United Kingdom • Bioinformatics and Functional Genomics, Centro de Investigación del Cáncer, Instituto de Biología Molecular y Celular del Cáncer, Consejo Superior de Investigaciones Científicas (CSIC)-Universidad de Salamanca, Campus Miguel de Unamuno, Salamanca, Spain • Inflammation and Macrophage Plasticity Lab, CIC bioGUNE, Derio, Spain • Oncogene Biology Laboratory, Francis Crick Institute, London, United Kingdom • Institute for Bioengineering of Catalonia (IBEC), The Barcelona Institute for Science and Technology (BIST), Barcelona, Spain • Ikerbasque, Basque Foundation for Science, Bilbao, Spain • Pathology Unit, Centro de Investigación del Cáncer, Instituto de Biología Molecular y Celular del Cáncer, Universidad de Salamanca, Campus Miguel de Unamuno, Salamanca, Spain

eLife Assessment

This **useful** study investigates the impact of disrupting the interaction of RAS with the PI3K subunit p110α in macrophage function in vitro and inflammatory responses in vivo. **Solid** data overall supports a role for RAS-p110α signalling in regulating macrophage activity and so inflammation, however for many of the readouts presented the magnitude of the phenotype is not particularly pronounced. Further analysis would be required to substantiate the claims that RAS-p110α signalling plays a key role in macrophage function. Of note, the molecular mechanisms of how exactly p110α regulates the functions in macrophages have not yet been established.

https://doi.org/10.7554/eLife.94590.2.sa3

Abstract

Macrophages are crucial in the body's inflammatory response, with tightly regulated functions for optimal immune system performance. Our study reveals that the RAS-p110α signalling pathway, known for its involvement in various biological processes and tumorigenesis, regulates two vital aspects of the inflammatory response in macrophages: the initial monocyte movement and later-stage lysosomal function. Disrupting this pathway, either in a mouse model or through drug intervention, hampers the inflammatory response, leading to delayed resolution and the development of more severe acute inflammatory reactions in live models. This discovery uncovers a previously unknown role of the p110α isoform in immune regulation within macrophages, offering insight into the complex mechanisms governing their function during inflammation. With emerging potential to activate p110α using small molecules, targeting the RAS-p110α pathway could be a promising approach for treating chronic inflammation. This therapeutic prospect holds significant promise for easing inflammatory disorders and improving the quality of life for affected patients.

Introduction

Phosphatidylinositol 3-kinases (PI3K) are a family of lipid kinases that phosphorylate phosphatidylinositides (PtdIns) at the 3'-hydroxyl group[1]. Upon activation, PI3K phosphorylates phosphatidylinositol 4,5-bisphosphate (PIP_2) to generate phosphatidylinositol 3,4,5-trisphosphate (PIP_3). PIP3 serves as a second messenger that recruits proteins containing pleckstrin homology (PH) domains, such as Akt (also known as protein kinase B)[2, 3]. This activation of PI3K regulate various cellular functions, including cell proliferation, growth, survival, motility, inflammation, and metabolism, among others[1, 4]. In macrophages, the activation of PI3K-Akt signalling is crucial to restrict inflammation and to promote anti-inflammatory responses in Toll Like Receptors (TLR)-induced macrophages, contributing to macrophage polarization[5, 6].

PI3Ks are heterodimeric lipid kinases composed of catalytic and adaptor/regulatory subunits that can be categorized into three classes based on their structures and substrate specificities[3,7]. Class I catalytic isoforms, including p110α, p110β, p110γ, and p110δ, play essential roles in integrating signals from growth factors, cytokines, and other environmental cues. While p110α and p110β are ubiquitously expressed, p110δ and p110γ are largely restricted to the myeloid and lymphoid lineages[7–9]. While p110α is primarily associated with cell growth regulation and survival in epithelial cells, it must be considered that this isoform is also expressed in immune cells, including macrophages. The role played by p110α in macrophages is not well understood, although some studies have suggested that it might regulate the survival and the regulation of the phagocytic activity of macrophages[10]. In the context of cancer, impairment of RAS binding to p110α in macrophages results in reduced recruitment of macrophages to the tumour site [11, 12]. Additionally, this disruption leads to a change in macrophage polarization, favouring a more proinflammatory M1 state [12]. These findings suggest that p110α plays a crucial role in regulating macrophage-dependent functions. However, despite these insights, the precise impact of p110α on macrophage function and the underlying molecular mechanisms influencing the inflammatory response are not yet fully understood.

Inflammation is a complex and tightly regulated series of events triggered by various stimuli such as pathogens, harmful mechanical and chemical agents, and autoimmune reactions. The inflammatory response primarily occurs in vascularized connective tissues, involving a dynamic interplay of plasma components, circulating cells, blood vessels, and cellular and extracellular

factors[13–17]. During inflammation, mediators released by recruited leukocytes orchestrate a response that aims to facilitate tissue repair and protect the body against harmful stimuli[16–18].

Macrophages play a vital role in the inflammatory response by performing functions such as antigen presentation, phagocytosis, and immunomodulation[16, 17]. Their role begin with the active recruitment of monocytes from the bloodstream to the site of infections[19] where they differentiate into macrophages and recognize microbes and cellular debris through specific mechanisms. Macrophages subsequently actively participate in phagocytosis, a vital process involving the internalization and elimination of pathogens. Microbial destruction predominantly takes place within lysosomes and phagolysosomes[20–23]. At later stages of inflammation, macrophages contribute to the resolution of inflammation, thus preventing progression from acute to persistent inflammation that would cause additional tissue damage.

In this study we have used a combination of cell biology techniques and animal models to better understand the role of RAS-dependent activation of p110α at the different stages of the inflammatory response. Our findings show that RAS-p110α signalling plays a key role in the initial stages of inflammation, facilitating the extravasation of monocytes from the bloodstream by promoting the necessary cytoskeletal changes. Subsequently, RAS-p110α has a crucial role in lysosomal acidification and activation of cathepsins, which are indispensable for efficient degradation of lysosomal cargo; when these functions are impaired, prolonged acute inflammatory responses and delayed resolution steps are observed. These results significantly enhance our understanding of the complex mechanisms governing the immune response to inflammation, emphasizing the pivotal role played by RAS-p110α signalling in orchestrating proper monocyte extravasation and maintaining optimal lysosomal function.

Results

Disruption of RAS-p110α causes prolonged and more acute responses to inflammatory stress *in vivo*

Previous data suggested that, in a tumoral setting, somatic disruption of RAS-p110α prevents macrophage recruitment to tumours[11, 12] and favours polarization of macrophages to a proinflammatory phenotype[12], suggesting a possible role for p110α in macrophage function. To determine whether RAS-dependent activation of p110α participates in innate or adaptive immune responses to inflammation in macrophages, we used an established mouse model designed for the tamoxifen-inducible disruption of RAS binding to p110α[11, 24] (**Supplementary Fig. S1A**). This mouse model introduces two-point mutations, T208D and K227A, in the RAS Binding Domain (RBD) of the endogenous Pik3ca allele ($Pik3ca^{RBD}$), enabling the selective disruption of the RAS-p110α interaction [24]. Wild-type ($Pik3ca^{WT}$) and $Pik3ca^{RBD}$ mice were bred with mice containing a floxed *Pik3ca* allele[25], along with a strain containing a conditional Cre recombinase (Cre-ERT2) allele targeted to the ubiquitously expressed Rosa26 locus. The resulting $Pik3ca^{WT/Flox}$ and $Pik3ca^{RBD/Flox}$ mice displayed no discernible phenotype and exhibited behavior consistent with $Pik3ca^{WT}$ mice[11, 24]. Activation of Cre-recombinase by tamoxifen led to the excision of the floxed *Pik3ca* allele, resulting in mice expressing either one $Pik3ca^{WT}$ allele ($Pik3ca^{WT/-}$) or one $Pik3ca^{RBD}$ allele ($Pik3ca^{RBD/-}$)[11]. This inducible genetic manipulation strategy allows us to selectively disrupt the RAS-p110α interaction in a controlled and temporally regulated manner, providing a valuable tool for dissecting the contributions of this pathway to immune responses in the context of inflammation.

Bone marrow derived macrophages (BMDMs) were generated from tibias and femurs of $Pik3ca^{WT/Flox}$ and $Pik3ca^{RBD/Flox}$ mice, ensuring efficient removal of the floxed allele (**Supplementary Fig. S1B**). Subsequently, these BMDMs were induced towards a

proinflammatory state through stimulation with LPS and IFN-γ. To assess the impact of RAS-p110α binding deficiency on inflammatory intracellular signalling, we first examined Akt activation. The results revealed a decrease in Akt activation levels under inflammatory conditions in BMDMs lacking RAS-p110α binding, while no discernible change was observed in ERK activation, another well-known RAS effector (**Fig. 1A and supplementary Fig. S1C and D**). Interestingly, the decrease in Akt activation was accompanied by a decrease in the activation of NF-κB (**Fig. 1B**).

Given the role of p65 in the expression of pro-inflammatory cytokines and chemokines[26] we next analyzed the expression of various inflammation mediators using a cytokine array in unstimulated and LPS- and IFN-γ-stimulated macrophages. Results showed that, under unstimulated conditions, RAS-PI3K disruption decreases the expression of IP-10, MIP-1α (Ccl3), JE (Ccl2/MCP1), IL-16, and IL-12p70, with no upregulated cytokines observed (**Supplementary Fig. S1E**). The downregulation of IP-10, MIP-1α, and JE indicates an impaired ability to recruit monocytes, macrophages, and T cells to sites of inflammation. This suggests that macrophages lacking RAS-PI3K interaction may have a reduced capacity to mount a robust immune response, particularly in recruiting and activating essential immune cells needed to combat pathogens or initiate inflammation.

Regarding LP +IFN-γ stimulated macrophages, results showed a decrease in the expression of IL-1β and IL-17, key drivers of pro-inflammatory responses, and an upregulation of IL-7, ILra, JE, BLC, I-309, Eotaxin, and G-CSF (**Supplementary Fig. S1F**). Elevated levels of these factors are associated with enhanced chemotactic signals and regulatory functions. Thus, the cytokine and chemokine expression profile observed in RAS-PI3K deficient macrophages suggests impaired pro-inflammatory responses and altered immune cell recruitment patterns, potentially influencing the resolution of inflammation and tissue repair processes.

Next we assessed whether the absence of RAS binding to p110α affects the ability of BMDMs to acquire a pro-inflammatory state characterized by increased expression of markers such as CD80, CD86, and MHCII[27, 28]. To assess this, *Pik3ca*$^{RBD/-}$and *Pik3ca*$^{WT/-}$ BMDMs were stimulated with LPS+IFN-γ, followed by flow cytometry analysis. Expression levels of CD80 (**Supplementary Fig. S1G**), CD86 (**Supplementary Fig. S1H**), and MCHII (**Supplementary Fig. S1I**) were examined. No significant differences were observed in the expression levels of any of these markers between the two genotypes under study.

Consequently, our next objective was to investigate whether in vivo disruption of RAS-p110α might lead to altered inflammatory responses. To address this, we administered tamoxifen to 10–12-week-old *Pik3ca*$^{WT/flox}$ and *Pik3ca*$^{RBD/flox}$ mice with tamoxifen and, after a two-week interval, conducted a paw swelling assay. In this assay, zymosan (10 μg/μl) or PBS was injected into the hind paws of *Pik3ca*$^{RBD/-}$ and *Pik3ca*$^{WT/-}$ mice with paw thickness measured at regular intervals over a 5-day period. The results revealed a significant increase in paw inflammation in *Pik3ca*$^{RBD/-}$ mice compared to *Pik3ca*$^{WT/-}$ mice, evident from the earlier time points measured and persisting throughout the experiment (**Fig. 1D and 1E**). Paws from the *Pik3ca*$^{WT/flox}$ and *Pik3ca*$^{RBD/flox}$ mice, which had not received tamoxifen, exhibited comparable levels of inflammation (**Supplementary Fig. S1J**). This reaffirms that the absence of p110α triggers a significant alteration in the inflammatory response and confirms that *Pik3ca*$^{WT/flox}$ and *Pik3ca*$^{RBD/flox}$ mice do not show any phenotype, as previously described[11, 24]. Additionally, analysis of the blood sedimentation rate, a reliable indicator of systemic inflammation levels[29], showed a lower basal sedimentation ratio in *Pik3ca*$^{RBD/-}$ mice under PBS-treated conditions (**Supplementary Fig. S1K**). Following zymosan injection, both genotypes exhibited an increase in sedimentation rate, but the rise was more pronounced in *Pik3ca*$^{RBD/-}$ mice, indicating a heightened systemic inflammatory response. These findings underscore that disruption of RAS-p110α interaction results in an exacerbated inflammatory state, reflected in both localized paw inflammation and systemic inflammatory mediator levels.

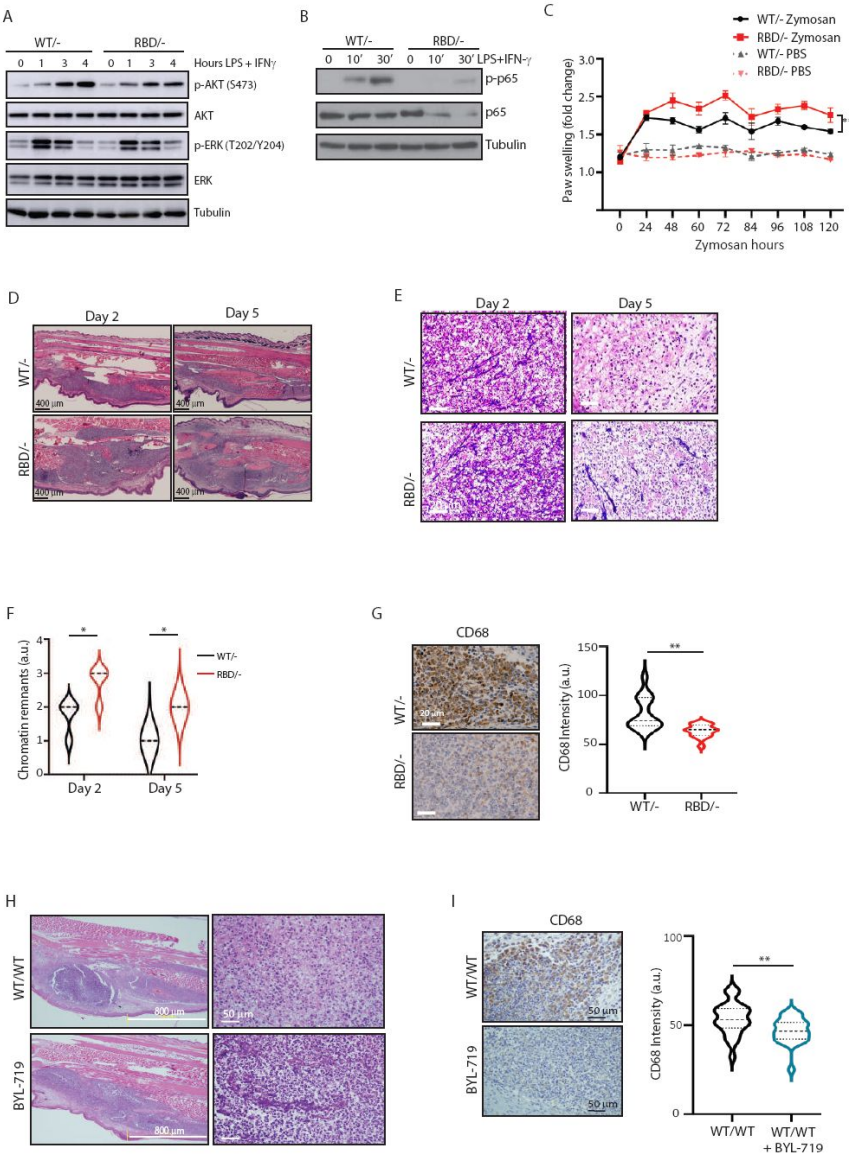

Figure 1.

Pik3ca$^{RBD/-}$ mice have impaired responses to inflammatory insults.

(A) Western blotting showing activation of Akt and ERK in *Pik3ca*$^{WT/-}$ and *Pik3ca*$^{RBD/-}$ BMDMs activated towards a pro-inflammatory state with LPS and IFN-γ at the indicated time points; **(B))** Western blotting showing activation of NF-κB (p65) in *Pik3ca*$^{WT/-}$ and *Pik3ca*$^{RBD/-}$ BMDMs activated towards a pro-inflammatory state with LPS and IFN-γ at the indicated time points; **(C)** *Pik3ca*$^{WT/-}$ and *Pik3ca*$^{RBD/-}$ mice were injected with zymosan or PBS in the back-hind paws and inflammation was measured and plotted over time, *Pik3ca*$^{WT/-}$ PBS n = 6; *Pik3ca*$^{RBD/-}$ PBS n = 5; *Pik3ca*$^{WT/-}$ Zymosan n = 4; *Pik3ca*$^{RBD/-}$ Zymosan n = 4; Error bars indicate mean ± SEM. Significance using 2-way ANOVA test: **p < 0.01 **(D)** Representative H&E images of the inflamed area of *Pik3ca*$^{WT/-}$ and *Pik3ca*$^{RBD/-}$ paws injected with zymosan at the indicated times; (**E**) Representative images of cellularity present in the inflamed abscess of *Pik3ca*$^{WT/-}$ and *Pik3ca*$^{RBD/-}$ paws injected with zymosan at the indicated times; **(F)** Graph showing quantification of loose chromatin present in the inflamed abscess; **(G)** Representative images of macrophages (CD68 positive cells) present in the inflamed abscess of *Pik3ca*$^{WT/-}$ and *Pik3ca*$^{RBD/-}$ paws injected with zymosan and quantification of macrophages (CD68 positive cells) present; (**H**) Representative H&E images of the inflamed area and cellularity of *Pik3ca*$^{WT/WT}$ paws and *Pik3ca*$^{WT/WT}$ paws treated with BYL-719 injected with zymosan. **(I)** Representative images and quantification of macrophages (CD68 positive cells) present in the inflamed abscess of *Pik3ca*$^{WT/WT}$ paws and *Pik3ca*$^{WT/WT}$ paws treated with BYL-719 injected with zymosan and quantification of macrophages (CD68 positive cells). Error bars indicate mean ± SEM. Significance using Student's t test: **p < 0.01.

To delve deeper into the inflammatory response induced by zymosan, we collected paw samples at two- and five-days post-injection and conducted Haematoxylin & Eosin (H&E) studies. This approach enabled a comprehensive analysis, allowing us not only to scrutinize the early stages of inflammation but also to monitor the subsequent resolution phase of the inflammatory process. Paws obtained from mice injected with zymosan for 2 days displayed extensive areas of damaged connective tissue in both *Pik3ca*$^{RBD/-}$ and *Pik3ca*$^{WT/-}$ paws (**Fig. 1D**). Notably, the inflamed region in *Pik3ca*$^{RBD/-}$ mice was larger compared to control samples. After 5 days of zymosan injection, there was a significant reduction in the inflamed area, although it remained comparatively larger in the paws from *Pik3ca*$^{RBD/-}$ mice (**Fig.1D**). This observation suggests a prolonged and heightened inflammatory response in mice lacking RAS-p110α interaction, emphasizing the role of this interaction in the regulation of inflammatory processes.

The cellular composition within the inflammatory abscess offers crucial insights into the severity and progression of the disease. Close examination with the pathologist revealed features indicative of an acute inflammatory response, including an inflammatory abscess with elevated numbers of polymorphonuclear cells, primarily neutrophils, and macrophages displaying altered cell shape and increased cell death, accompanied by fibrin and chromatin deposition (**Fig. 1E and F**). Notably, *Pik3ca*$^{RBD/-}$ mice exhibited lower numbers of macrophages, a larger necrotic area with increased chromatin remnants, and reduced fibrin content compared to the paws from *Pik3ca*$^{WT/-}$ mice (**Fig. 1E and F**). By day 5, paws from *Pik3ca*$^{WT/-}$ mice showed a significant increase in the number of macrophages, a decrease in polymorphonuclear cells, and a nearly complete resolution of the necrotic area, indicating the initiation of the resolution phase. Moreover, there were abundant activated fibroblasts), suggesting active production of new connective tissue. In contrast, paws from *Pik3ca*$^{RBD/-}$ mice exhibited a delayed healing process characterized by a larger central area of polymorphonuclear cells, abundant fibrin deposits, reduced numbers of infiltrating macrophages, and limited fibroblast activity (**Fig. 1E and F**). These findings collectively indicate an imbalance in the inflammatory response and a slower progression towards resolution in the absence of RAS-p110α interaction, emphasizing the pivotal role of this interaction in orchestrating an effective and timely resolution of inflammation.

To evaluate the presence of macrophages within the inflammatory lesion, we performed specific immunohistochemical (IHC) analysis using the macrophage-specific marker CD68 in paws from day 5, where more cellular preservation and initiation of the healing process had been observed. A notable decrease in the number of CD68-positive cells was observed in the inflamed abscess region of *Pik3ca*$^{RBD/-}$ mice (**Fig. 1G**).

To further confirm the involvement of p110α signalling in the acute inflammatory response, *Pik3ca*$^{WT/WT}$ mice were subjected to daily treatment with BYL719 (Alpelisib), a specific inhibitor of p110α isoform. After an initial 48-hour treatment period, the mice received injections of zymosan or PBS into their back-hind paws and were sacrificed 2 days later for analysis. Similar to what we had observed in *Pik3ca*$^{RBD/-}$mice, the inflamed area in BYL719-treated mice exhibited a larger extension than the inflamed are from non-treated mice (**Fig. 1H and Supplementary Fig. S1L**). The central necrotic region was significantly larger in the BYL719-treated mice, and it contained large amount of apoptotic polymorphonuclear cells, lower number of macrophages, and increased deposits of chromatin (**Fig. 1H**) resembling the observations from *Pik3ca*$^{RBD/-}$ mice. Immunostaining for CD68 revealed a reduction in the number of macrophages present in the inflammatory abscess upon inhibition of p110α signalling with BYL719 treatment (**Fig. 1I**).

In summary, our findings highlight that both genetic disruption of RAS-p110α interaction and pharmacological inhibition of p110α contribute to an expanded inflamed area and central necrotic region, concurrently reducing macrophage infiltration in a zymosan-induced inflammation model. These results collectively underscore the pivotal role of the p110α isoform of PI3K in orchestrating the resolution of inflammatory responses, emphasizing its significance in modulating the dynamics and outcomes of inflammatory processes.

Disruption of RAS binding to p110α impairs the number of inflammatory monocytes in blood and spleen

Given the decrease in macrophages observed in the inflammatory abscess, we next set out to determine whether disruption of RAS binding to p110α had an effect on the number of monocytes circulating in the blood of adult mice. *Pik3ca*$^{WT/flox}$ and *Pik3ca*$^{RBD/flox}$ mice were treated with tamoxifen at 12–14 weeks of age and 4 weeks later, blood was collected by cardiac puncture and immune populations were analysed by flow cytometry. We found a decrease in the number of circulating classical (or inflammatory) monocytes (Ly6C^{Hi}/Ly6G^{-}/CD11b^{+} cells) in *Pik3ca*$^{RBD/-}$ mice (**Fig. 2A**) and no changes were observed in non-classical (or non-inflammatory) monocytes (Ly6C^{Lo}/Ly6G^{-}/CD11b^{+} cells) (**Fig. 2B**). Together with the decrease in inflammatory monocytes, we observed an increase in the number of neutrophils (Ly6C^{-}/Ly6G^{+}/CD11b^{+} cells) (**Supplementary Fig. S2A**). We did not detect differences in the numbers of T-cells (CD3^{+}, CD8^{+} or CD4^{+}) (**Supplementary Fig. S2B**) or B-cells (CD19^{+}) (**Supplementary Fig. S2C**) in the blood after the disruption of RAS binding to p110α. We also analysed these same cell populations in *Pik3ca*$^{WT/flox}$ and *Pik3ca*$^{RBD/flox}$ mice and no differences were found (data not shown).

Since splenic monocytes resemble their blood counterparts[30] we next aimed at determining whether splenic monocyte population would also be altered after disruption of RAS p110α interaction. As observed in circulating blood, the number of classical monocytes (Ly6C^{Hi}/Ly6G^{-}/CD11b^{+}) in the spleen decreased after disruption of RAS-p110α interaction (**Fig. 2C**) and no differences were found in non-classical activated monocytes (Ly6C^{Lo}/ Ly6G^{-}/CD11b^{+}) (**Fig. 2D**). We also checked the levels of resident macrophages present in the spleen and results showed that spleens from the *Pik3ca*$^{RBD/-}$ mice had a decrease in the number of differentiated macrophages (F4/80^{+}/CD11b^{+}/CD45^{+}) (**Fig. 2E**). Analysis of macrophages in the white and red pulp of the spleen indicated that *Pik3ca*$^{RBD/-}$ mice had a significant decrease in the macrophage population in the former region (**Fig. 2F and 2G**). No differences were found in the number of granulocytes (**Supplementary Fig. S2D**), B-cells (**Supplementary Fig. S2E**) or T-cells (**Supplementary Fig. S2F**) present in the spleen between *Pik3ca*$^{RBD/-}$ and *Pik3ca*$^{WT/-}$ mice. There were no differences in spleen size from *Pik3ca*$^{RBD/-}$ and *Pik3ca*$^{WT/-}$ mice either (**Supplementary Fig. S2G**).

Given the decrease in the number of inflammatory monocytes and macrophages observed in blood and spleens of *Pik3ca*$^{RBD/-}$ mice, we wondered if disruption of RAS activation of p110α could lead to a decrease in myeloid bone marrow precursors. Myeloid lineage descends from a common myeloid progenitor (CMP) in bone marrow and traverse into blood as mature cells[31]. CMP differentiates into the Granulocyte-Macrophage Progenitor (GMP) and the Megakaryocyte-Erythroid Progenitor (MEP). The CMP can generate all types of myeloid colonies, whereas the GMP or the MEP produces only granulocyte macrophage (GM) or megakaryocyte erythrocyte (MegE) lineage cells, respectively (**Supplementary Fig. S2H**). No significant differences were noted in the quantity of CMP progenitors within the bone marrow *Pik3ca*$^{RBD/-}$ and *Pik3ca*$^{WT/-}$ mice (**Supplementary Fig. S2I-L**). This observation suggests that the variations observed in blood and spleen parameters are not attributable to impairments in progenitor fate.

Finally, bone marrow precursors from *Pik3ca*$^{RBD/flox}$ and *Pik3ca*$^{WT/flox}$ mice were differentiated into macrophages *in vitro*, and the number of bone marrow-derived macrophages (BMDM) was determined by flow cytometry analysis. No differences were found in the number of BMDMs obtained from *Pik3ca*$^{RBD/-}$ and *Pik3ca*$^{WT/-}$ mice (**Supplementary Fig. S2M**), suggesting that the disruption of RAS-p110α signalling do not interfere with the ability of bone marrow precursors to differentiate to macrophages.

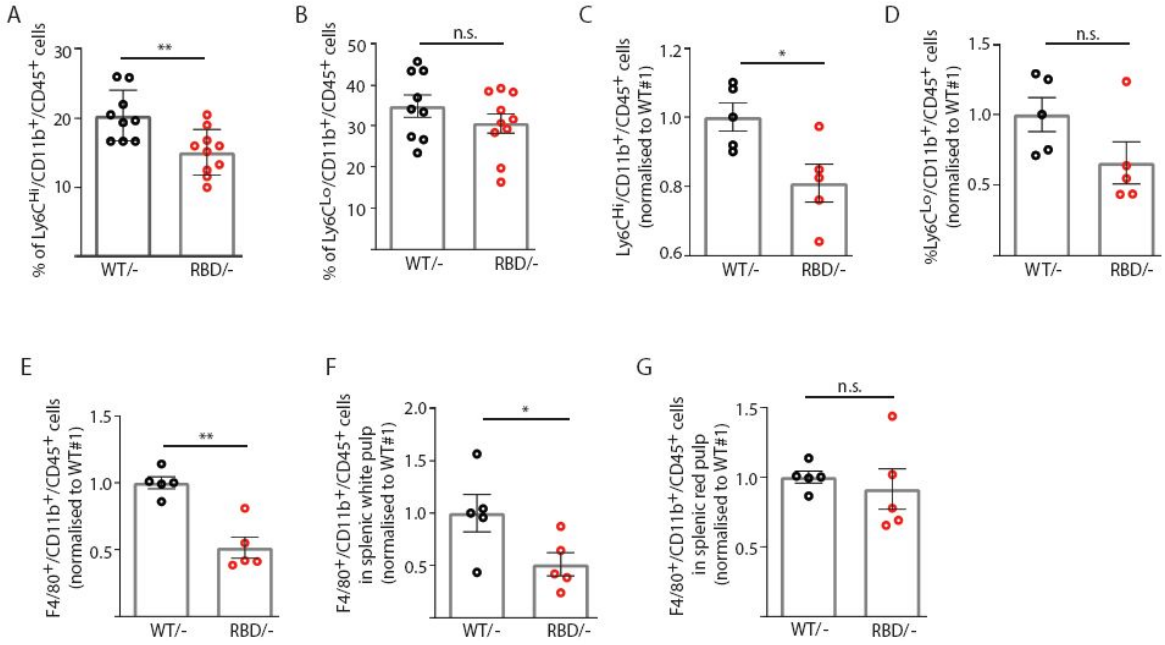

Figure 2.

Disruption of RAS-p110α interaction decreases the number of inflammatory monocytes in blood and spleen.

Twelve-week-old mice were treated with tamoxifen and after four weeks, flow cytometry analysis was performed to determine **(A)** inflammatory monocytes in circulating blood; **(B)** alternatively activated monocytes in circulating blood; **(C)** inflammatory monocytes in spleen; **(D)** classically activated monocytes in spleen; **(E)** macrophages in spleen; **(F)** macrophages in spleen's white pulp; (**G**) macrophages in spleen's red pulp. Data are presented as percentage of positive cells for the indicated markers. Black dots represent data from *Pik3ca*$^{WT/-}$ mice and red dots represent data from *Pik3ca*$^{RBD/-}$ mice. Each dot represents an individual mouse. Error bars indicate mean ± SEM. Significance using Student's t test: * $p < 0.05$; ** $p < 0.01$.

Disruption of RAS binding to p110α impairs monocyte transendothelial extravasation in response to inflammatory cues

The decrease in classical monocytes observed in the inflammatory abscess of paws from *Pik3ca*$^{RBD/-}$ mice may indicate a decreased ability to mount an effective immune response. We carried out transwell assays since they are widely used to quantify transendothelial migration. Fibroblasts were seeded in the lower chamber to provide a continuous supply of Ccl2[32], as this cytokine is well known for its ability to drive chemotaxis of myeloid cells under inflammatory conditions[33]. *Pik3ca*$^{RBD/-}$ or *Pik3ca*$^{WT/-}$ BMDMs were seeded in the upper chamber of the transwell. Additionally, we stimulated *Pik3ca*$^{RBD/-}$ or *Pik3ca*$^{WT/-}$ BMDMs with lipopolysaccharide (LPS) and Interferon gamma (IFN-γ) to mimic/recapitulate the proinflammatory phenotype typically associated with bacterial infection that causes macrophage activation[34]. Results showed that in both unstimulated and LPS+IFN-γ stimulated BMDMs, a lower number of *Pik3ca*$^{RBD/-}$ BMDMs were able to go through the trans-well pore membranes compared to *Pik3ca*$^{WT/-}$ BMDMs (**Fig. 3A**). As expected, when BMDMs were stimulated towards a proinflammatory phenotype, a decrease in their migratory ability is observed[35].

Extravasation entails the migration of monocytes through the endothelium[36, 37], so we conducted random migration assays of *Pik3ca*$^{RBD/-}$ and *Pik3ca*$^{WT/-}$ BMDMs growing in matrigel coated plates under unstimulated conditions or activated towards an inflammatory phenotype by addition of LPS and IFN-γ to the media. Analysis of the data revealed that, under pro-inflammatory conditions, *Pik3ca*$^{RBD/-}$ BMDMs displayed a decrease in migration speed (**Fig. 3B**). Migration was also evaluated in *Pik3ca*$^{WT/WT}$ BMDMs treated with BYL-719. Results confirmed a decrease in migration speed of macrophages upon treatment with BYL-719 (**Fig. 3B**) indicating that inhibition of p110α, either genetically or pharmacologically, reduces the ability of macrophages to migrate under inflammatory conditions.

To determine if disruption of RAS binding to p110α impairs monocyte ability to extravasate through the endothelium *in vivo* in response to an inflammatory stress, we analysed monocyte extravasation through the mesenteric vein in response to intraperitoneal Ccl2 injection. It is well established that loss of p110α function leads to significant impairment in endothelial and lymphatic system[12, 38], so in order to determine if monocytes from *Pik3ca*$^{RBD/-}$ mice presented an alteration in extravasation, we generated chimeric mice in which only the bone marrow were defective in RAS binding to p110α (**Fig. 3C**). For this, bone marrow from *Pik3ca*$^{RBD/-}$ or *Pik3ca*$^{WT/-}$ mice was injected through the tail vein of irradiated LysM-GFP donor mice[39]. Engraftment of *Pik3ca*$^{RBD/-}$ and *Pik3ca*$^{WT/-}$ bone marrow could be followed by disappearance of the eGFP signal in donor mice (**Fig. 3D** and **Supplementary Fig. S3A**). Neutrophils (but no monocytes) were depleted using an anti-GR1 antibody (**Fig. 3E** and **Supplementary Fig. S3B**) to avoid interference with monocyte extravasation. Intraperitoneal injection of Ccl2 was performed in the peritoneum of the chimera mice to induce extravasation of monocytes through the mesenteric vein and rolling, adhesion and extravasation was measured by intravital microscopy. Flow cytometry analysis demonstrated no differences in Ccr2 expression between *Pik3ca*$^{RBD/-}$ and *Pik3ca*$^{WT/-}$ monocytes (**Supplementary Fig. S3C**). We observed that blocking RAS-p110α interaction did not induce a decrease in the number of rolling monocytes (**Fig. 3F**) or in the number of monocytes that adhere to the endothelium (**Fig. 3G**). However, when extravasation was measured, data showed that disruption of RAS binding to p110α caused a significant decrease in the number of monocytes that were capable of extravasating through the endothelium of the mesenteric vein (**Fig. 3H**).

Additionally, in order to determine whether the differences observed in the inflammatory response of *Pik3ca*$^{RBD/-}$ mice were due to lack of monocyte extravasation, we repeated the zymosan paw swelling assay in the chimera mice. As previously, we observed that disruption of

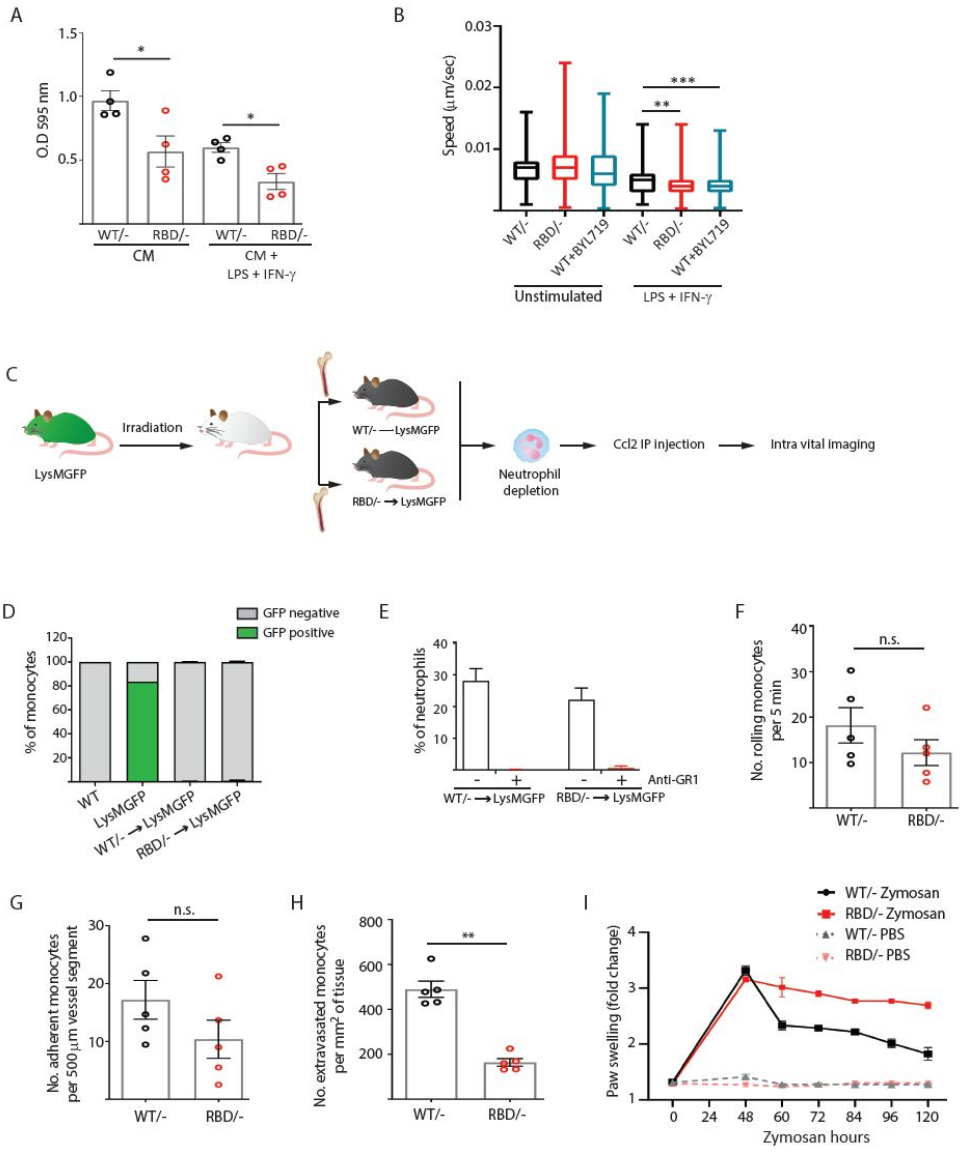

Figure 3.

Disruption of RAS-p110α interaction impairs transendothelial extravasation to sites of inflammation.

(**A**) Graph indicating the quantification of *Pik3ca*$^{RBD/-}$ and *Pik3ca*$^{RBD/-}$ BMDMs passing through 8 μm membrane pore transwells for 24 hours. Membrane attached macrophages on the lower part of the transwell were stained with crystal violet and quantified. Each dot represents an independent experiment. Error bars indicate mean ± SEM; (**B**) Random migration of *Pik3ca*$^{WT/-}$, *Pik3ca*$^{RBD/-}$ and *Pik3ca*$^{WT/WT}$ BMDMs treated with BYL719 (500 ng/ml) was analysed by time-lapse video microscopy and cell tracing in the presence or absence of LPS (100 ng/ml) and IFN-γ (20 ng/ml); (**C**) Schematic representation of myeloid chimera generation strategy; (**D**) Graph showing level of bone marrow reconstitution with *Pik3ca*$^{RBD/-}$ and *Pik3ca*$^{WT/-}$ myeloid lineage; (**E**) Graph quantifying the number of neutrophils in the blood of chimera mice treated with anti-GRl (25μg/mouse/day); (**F-H**) Intra vital imaging quantification of the number of: (**F**) rolling monocytes per 5 minutes; (**G**) adherent monocytes per 500 μm of vessel segment; (**H**) extravasated monocytes per mm^2 of tissue. Each dot represents an individual mouse. **(I)** Chimera *Pik3ca*$^{WT/-}$ and *Pik3ca*$^{RBD/-}$ mice were injected with zymosan or PBS in the back-hind paws and inflammation was measured and plotted over time, *Pik3ca*$^{WT/-}$ PBS n = 5; *Pik3ca*$^{RBD/-}$ PBS n = 5; *Pik3ca*$^{WT/-}$Zymosan n = 5; *Pik3ca*$^{RBD/-}$ Zymosan n = 5.

Statistical significance was obtained using Mann-Whitney test (A-H) or 2-way ANOVA test (I): n.s. nonsignificant; *p < 0.05; **p < 0.01; ***p < 0.001; ****p < 0.0001.

RAS-p110α only in the immune system led to higher inflammatory response and a delay in the initiation of the resolution phase (**Fig. 3I**).

Disruption of RAS-p110α activation in macrophages induces changes in cytoskeleton reorganization

During transendothelial migration, leukocytes undergo cytoskeletal rearrangements that allow them to squeeze through the tight spaces between endothelial cells and enter the underlying tissue[40, 41]. Therefore, we next sought to determine whether the differences observed in *Pik3ca*$^{RBD/-}$ BMDMs extravasation and migration were attributable to altered cytoskeletal dynamics. To do so, we first aimed at examining cell shape and spread in *Pik3ca*$^{RBD/-}$ and *Pik3ca*$^{WT/-}$ BMDMs in pro-inflammatory conditions after LPS+IFN-γ treatment. Treatment with LPS+IFNγ induced an increase in cell spread in both *Pik3ca*$^{RBD/-}$ and *Pik3ca*$^{WT/-}$ BMDMs when compared to their respective unstimulated counterparts (**Fig. 4A and 4B**). However, cell spread in LPS+IFNγ activated *Pik3ca*$^{RBD/-}$ BMDMs was significantly decreased compared to that observed *Pik3ca*$^{WT/-}$ BMDMs (**Fig. 4A and 4B**). Additionally, *Pik3ca*$^{RBD/-}$ BMDMs were more elongated and did not acquire the typical rounded shape known to be induced in macrophages after treatment with LPS+IFN-γ[42] (**Fig. 4A and 4C**). We also analysed cell height and results showed that *Pik3ca*$^{RBD/-}$ BMDMs are higher both in unstimulated conditions and after LPS+IFN-γ stimulation (**Fig. 4D**).

Actin is a bona fide regulator of cell shape[43], so we next aimed at exploring the actin cytoskeleton in *Pik3ca*$^{RBD/-}$ and *Pik3ca*$^{WT/-}$ BMDMs. Actin fractionation assays were carried out in unstimulated or LPS+IFNY activated *Pik3ca*$^{RBD/-}$ and *Pik3ca*$^{WT/-}$ BMDMs. Our results revealed that disruption of RAS-p110α binding caused a decrease in the F-actin pool in unstimulated BMDMs (**Fig. 4E**), with no changes observed in the G-actin pool when compared to matched controls (**Fig. 4F**). Analysis of actin dynamics after activation with LPS+IFNγ showed that, in proinflammatory conditions, the F-actin pool is increased, as expected[44] (**Fig. 4E**). However, actin polymerization was significantly active in *Pik3ca*$^{RBD/-}$ BMDMs, leading to a striking increase in F-actin when compared to that observed in controls (**Fig. 4E**). In parallel, a decrease in the G-actin pool in *Pik3ca*$^{RBD/-}$ BMDMs was observed, suggesting an increase in the stabilization of F-actin after disruption of RAS binding to p110α (**Fig. 4F**).

We next sought to investigate whether the enhanced F-actin stabilization corresponded to increased cellular rigidity. Consequently, we measured the elastic modulus of *Pik3ca*$^{RBD/-}$ BMDMs, revealing a significant increase in cell stiffness following RAS-p110α disruption under both basal and proinflammatory conditions (**Fig. 4G**). To validate that the heightened cell stiffness was attributed to p110α, we treated *Pik3ca*$^{WT/WT}$ BMDMs with BYL-719 and observed an amplified elastic modulus in these cells when stimulated with LPS+IFN-γ (**Fig. 4G**), confirming that the inhibition of p110α indeed results in augmented cellular rigidity.

These observations led us to hypothesize that phagocytosis, which heavily relies on actin rearrangement, might also be affected in *Pik3ca*$^{RBD/-}$ BMDMs. To test this hypothesis, we assessed the ability of *Pik3ca*$^{RBD/-}$ and *Pik3ca*$^{WT/-}$ BMDMs to phagocytose fluorescent microspheres, Borrelia burgdorferi, and apoptotic cells. The results revealed varying outcomes depending on the target. When phagocytosing 1 μm non-opsonized green-fluorescent beads, *Pik3ca*$^{RBD/-}$ BMDMs were less efficient at engulfing the microspheres compared to their WT counterparts (**Supplementary Fig. S4A**). Similar results were obtained when *Pik3ca*$^{WT/WT}$ BMDMs were treated with BYL-719 (**Supplementary Fig. S4A**). In contrast, no significant differences were observed between *Pik3ca*$^{RBD/-}$ and *Pik3ca*$^{WT/-}$ BMDMs in their ability to phagocytose Borrelia burgdorferi (**Supplementary Fig. S4B**).

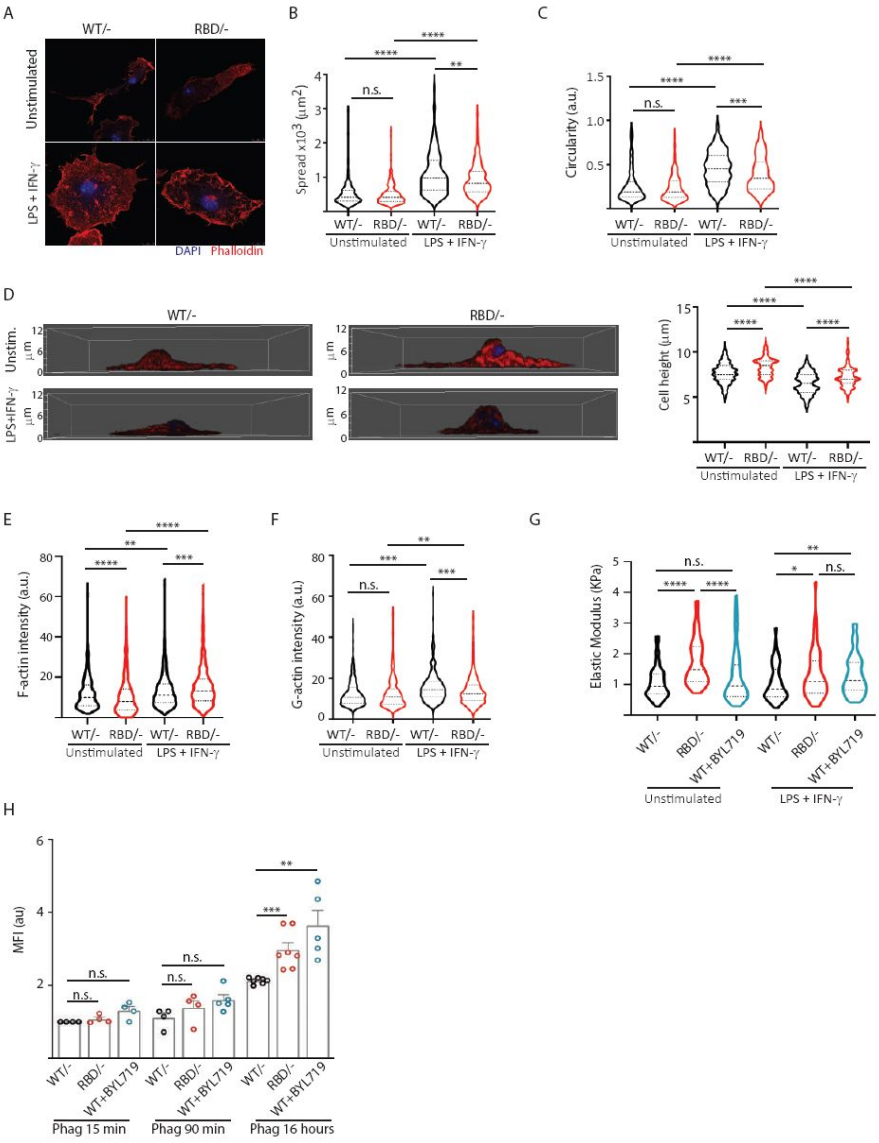

Figure 4.

Disruption of RAS-p110α signalling impairs BMDM ability to remodel their cytoskeleton in response to inflammatory cues.

(**A**) Representative images of *Pik3ca*$^{WT/-}$ and *Pik3ca*$^{RBD/-}$ BMDMs unstimulated or activated with LPS+ IFN-γ; **(B)** violin plot quantifying spread area. IF images of *Pik3ca*$^{WT/-}$ and *Pik3ca*$^{RBD/-}$ BMDMs co-stained with phalloidin and DAPI were used to analyse spread area. Results are represented as a violin plot. Three independent biological replicates were analysed (n ≥ 250 total cells); (**C**) Quantification of cell circularity of *Pik3ca*$^{WT/-}$ and *Pik3ca*$^{RBD/-}$ BMDMs unstimulated or activated with LPS+ IFN-γ. Quantification was performed using the same images from panel (A); (**D**) Representative 3D projections of *Pik3ca*$^{WT/-}$ and *Pik3ca*$^{RBD/-}$ BMDMs unstimulated or activated with LPS+IFN-γ and violin plot showing quantification of the corresponding cell height. 3D projections and cell height were analysed using same images used in panel (A). (**E**) Violin plot representing F-actin pool in *Pik3ca*$^{WT/-}$ and *Pik3ca*$^{RBD/-}$ BMDMs unstimulated or activated with LPS+ IFN-γ. Three independent biological replicates were analysed (n ≥ 250 total cells); (**F**) Violin plot representing G-actin pool (measured by DNAse staining) in *Pik3ca*$^{WT/-}$ and *Pik3ca*$^{RBD/-}$ BMDMs unstimulated or activated with LPS+ IFN-γ. Three independent biological replicates were analysed (n > 250 total cells); (**G**) Graph showing stiffness (elastic modulus) of *Pik3ca*$^{WT/-}$ and *Pik3ca*$^{RBD/-}$ BMDMs; **(H)** Graph showing phagocytosis of apoptotic cells (efferocytosis) over time in *Pik3ca*$^{WT/-}$, *Pik3ca*$^{RBD/}$ and *Pik3ca*$^{WT/WT}$ BMDMs treated with BYL719 BMDMs.

Statistical significance was obtained using Mann-Whitney test: n.s. non-significant; *p < 0.05; **p < 0.01; ***p < 0.001; ****p < 0.0001.

Lastly, we evaluated the phagocytosis of apoptotic cells by *Pik3ca*$^{RBD/-}$ BMDMs over extended periods. There were no differences in the initial uptake of apoptotic cells between *Pik3ca*$^{RBD/-}$and *Pik3ca*$^{WT/-}$ BMDMs. However, at later time points, *Pik3ca*$^{RBD/-}$ BMDMs showed an accumulation of phagocytosed particles. Similar results were obtained when *Pik3ca*$^{WT/WT}$ BMDMs were treated with BYL-719. These data suggest a delay in processing and degradation, indicating a potential role for RAS-p110α in the later stages of phagocytosis (**Fig. 4H**).

In summary, our findings suggest that loss of RAS-p110α interaction leads to increased actin polymerization, resulting in stiffer and less deformable cells, which impairs phagocytic efficiency for certain targets. Specifically, RAS-p110α is important for the effective phagocytosis of non-biological particles and may also play a role in the proper processing and degradation of phagocytosed apoptotic cells. The differential effects on various phagocytic targets highlight the complexity of RAS-p110α's role in macrophage biology and underscore the importance of cytoskeletal flexibility in efficient phagocytosis.

Disruption of RAS-p110α activation impacts the secretome of macrophages

Given our previous observations, we hypothesized that the cytoskeletal alterations observed after disruption of RAS-p110α interaction, may significantly impact the secretory functions of macrophages. The accumulation of apoptotic material in *Pik3ca*$^{RBD/-}$ BMDMs suggests a disruption in normal phagocytic processing, which could influence the release of cytokines and other inflammatory mediators. Thus, we analysed the secretome of *Pik3ca*$^{RBD/-}$ and *Pik3ca*$^{WT/-}$ BMDMs both under steady state condition and during phagocytosis. We utilized apoptotic LKR10 cells, a murine lung cancer cell line, as the substrate in our phagocytosis assay. LKR10 cells were exposed to cisplatin for 16 h and apoptosis was confirmed by Western Blot (**Supplementary Fig. S5A**). Our goal was to create a more physiologically relevant experimental setting that more closely mimics the complex nature of the inflammatory response. For the secretome analysis, macrophages were incubated with or without apoptotic cells for 16 h. Culture supernatants were collected, clarified, and subjected to label-free quantitative proteomics analysis.

A total of 127 peptides corresponding to 105 proteins (**Supplementary Table 1**) showed differential expression between *Pik3ca*$^{RBD/-}$ and *Pik3ca*$^{WT/-}$ BMDM secretomes at steady state conditions. Additionally, 359 peptides corresponding to 210 proteins (**Supplementary Table 2**) were present a significantly different levels in the secretomes of *Pik3ca*$^{RBD/-}$ and *Pik3ca*$^{WT/-}$ BMDM during phagocytosis of apoptotic cells. Next, we compared these peptides with the list of secreted proteins available at The Human Protein Atlas, and removed those that do not correspond to secreted proteins. After this step, 18 proteins were found to be differentially secreted by *Pik3ca*$^{RBD/-}$ and *Pik3ca*$^{WT/-}$ BMDM in steady state conditions (**Fig. 5A**), and 38 by *Pik3ca*$^{RBD/-}$ and *Pik3ca*$^{WT/-}$ BMDM during phagocytosis (**Fig. 5B** and **Supplementary Fig. S5B and S5C**). Surprisingly, most proteins were secreted at lower levels in *Pik3ca*$^{RBD/-}$ BMDMs, independently of the conditions under study. 12 proteins were differentially secreted in both experimental conditions under study (**Fig. 5C**).

Functional analysis of differentially secreted proteins in unstimulated BMDMs showed no significant pathways related to these group of proteins (**Fig. 5D**). However, differentially secreted proteins in phagocytosing conditions were involved in two main biological processes: complement activation (C1qa, C1qb and C1qc connected through physical interaction and C3, C9 and Cfb through coexpression) and lysosome function, mainly cathepsins (Ctsd, Ctsb, Ctsz, Cst3, Psap, Anxa1 and Gsn) (**Fig. 5E**). Together, the complement cascade and lysosome function work in concert to provide an effective defence against pathogens and promote overall maintenance of cellular homeostasis[22, 45–47] and data from the secretome analysis of *Pik3ca*$^{RBD/-}$ and *Pik3ca*$^{WT/-}$ BMDMs suggests that RAS activation of p110α may play a crucial role in the regulation

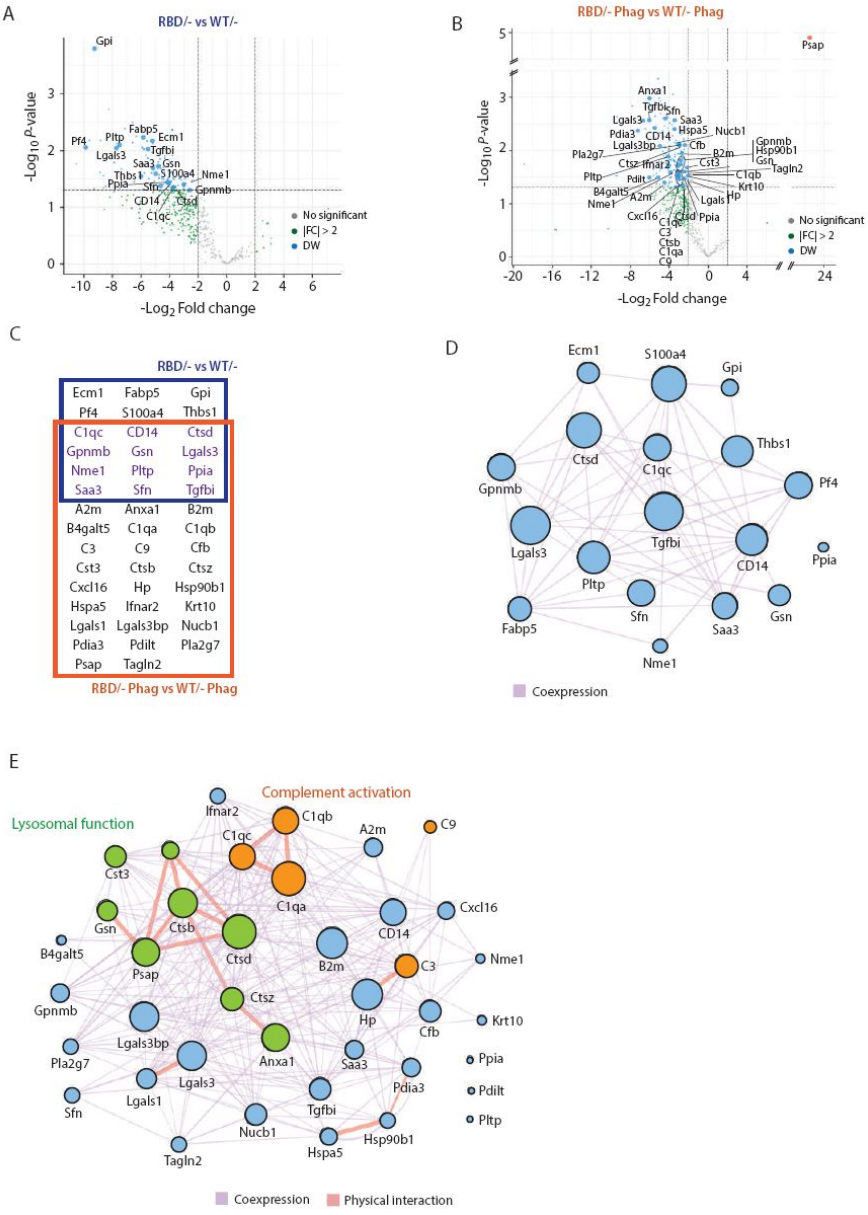

Figure 5.

Secretome analysis of *Pik3ca*$^{RBD/-}$ BMDMs suggested a defect in complement activation and lysosomal function.

(A and **B)** Volcano plots of secretome analysis from *Pik3ca*$^{WT/-}$ and *Pik3ca*$^{RBD/-}$ BMDMs in nonstimulated conditions (A) or phagocytosing apoptotic cells (B). The x-axis shows the log2 FC of each identified protein and the y-axis the corresponding -log10 P value. Statistically significant peptides with FC ≥2 and p-value < 0.05 are in blue; peptides that do not pass this threshold are in grey; peptides with FC ≥ 2 but p-value ≥ 0.05 are in green; (**C**) Venn diagram showing the overlap of *Pik3ca*$^{RBD/-}$ vs *Pik3ca*$^{WT/-}$ BMDMs differentially expressed proteins at rest and during phagocytosis of apoptotic cells. Proteins displayed in the blue square represents peptides differentially expressed in resting BMDMs, the brown square represents peptides differentially expressed during phagocytosis, and the peptides differentially expressed in both conditions are displayed in purple; (**D** and **E**) Network analysis of significantly expressed proteins identified in the secretome analysis of *Pik3ca*$^{RBD/-}$ vs *Pik3ca*$^{WT/-}$ BMDMs in steady state conditions (D) or during phagocytosis of apoptotic cells (E). The nodes represent individual proteins, and the edges represent known interactions between proteins, either coexpression (purple) or physical interaction (thick pink). The size of each node reflects the significance of differential expression. Proteins in green have been implicated in lysosomal function, while proteins in orange are members of the complement cascade.

of both response pathways. Moreover, these findings align with previous observations showing an accumulation of phagocytosed material in *Pik3ca*$^{RBD/-}$ BMDMs, indicating a potential disruption in the processing and degradation of engulfed targets.

Disruption of RAS-p110α signalling leads to altered lysosomal function

We next aimed to functionally validate the proteomics data suggesting that RAS-p110α activation regulates lysosomal function in macrophages. First, we performed immunofluorescence analysis of lysosomal-associated membrane protein 1 (LAMP1) to assess lysosomal biogenesis and function in *Pik3ca*$^{RBD/-}$ and *Pik3ca*$^{WT/-}$ BMDMs. Analysis of LAMP1 in *Pik3ca*$^{RBD/-}$ and *Pik3ca*$^{WT/-}$ BMDMs showed a decrease in LAMP1 expression in steady state conditions (**Fig. 6A**) suggesting a decrease in the number of lysosomes after disruption of RAS-p110α interaction. However, *Pik3ca*$^{RBD/-}$ showed increased levels of Lamp1 expression when subjected to phagocytosis of apoptotic cells, suggesting an increase in the number of phagolysosomes present in these cells.

We hypothesised that the increase in Lamp1 expression in BMDMs lacking RAS-p110α interaction during phagocytosis could be attributed to aberrant lysosomal function and phagolysosome retention. Thus, we next evaluated lysosomal activity by using the lysosomotropic dye lysotracker red coupled with epifluorescence analysis, since it is specifically taken up by acidic organelles. As such, its accumulation is proportional to the number of acidic vesicles. Data analysis showed that disruption of RAS-PI3K in BMDMs leads to a significant decrease in lysotracker uptake, both in unstimulated conditions and also after activation with LPS+IFN-γ (**Fig. 6B**). Similar results were obtained with control BMDMs treated with BYL719, the p110α specific inhibitor. Data analysis showed a decrease in the uptake of lysotracker after p110α inhibition (**Fig. 6B**), further suggesting that loss of p110α function in BMDMs results in altered lysosomal pH. To confirm that lysosomal pH of *Pik3ca*$^{RBD/-}$ BMDMs was less acidic, we next stained *Pik3ca*$^{RBD/-}$ and *Pik3ca*$^{WT/-}$ BMDMs with Green lysosensor, a pH-sensitive dye that exhibit a pH-dependent increase in fluorescent intensity upon lysosomal acidification. As shown in **Fig. 6C**, *Pik3ca*$^{RBD/-}$ BMDMs presented attenuated fluorescent intensity both in unstimulated and activated when compared with that in the control group, indicating that their lysosomal content is less acidic than in *Pik3ca*$^{WT/-}$ BMDMs.

Considering that *Pik3ca*$^{RBD/-}$ lysosomes were less acidic, we next investigated the expression level and activation of some of the cathepsins identified in the secretome analysis (**Fig. 5**) by western blotting. Cathepsins play a critical role in lysosomal protein degradation. They are initially synthesized as inactive precursors and are activated through proteolysis in the lysosome at a low pH[48]. We found a reduction in the expression and activation of cathepsin D and cathepsin B in *Pik3ca*$^{RBD/-}$ BMDMs upon stimulation with LPS+IFN-γ (**Figure 6D**). This observation suggests that the impaired lysosomal pH observed in *Pik3ca*$^{RBD/-}$ BMDMs could potentially account for the observed decrease in cathepsin activity.

Acidification of lysosomes and cathepsin activation are critical steps for activation of the resolutive stage of the inflammatory response, so we next evaluated the ability of *Pik3ca*$^{RBD/-}$ BMDM's lysosomal compartment to degrade internalised particles. We set up another phagocytosis assay in which *Pik3ca*$^{RBD/-}$ and *Pik3ca*$^{WT/-}$ BMDMs would phagocytose apoptotic cells that were transduced with GFP (which is pH sensitive[49]) and also labelled with Celltracker Red CMTPX (pH insensitive). *Pik3ca*$^{RBD/-}$ and *Pik3ca*$^{WT/-}$ BMDMs were allowed to engulf these apoptotic cells for 16 h and after this time, apoptotic cells were eliminated by washes and BMDMs were analysed by flow cytometry at different time points to measure GFP signal. Our results showed that GFP signal is lost significantly faster in control BMDMs than in *Pik3ca*$^{RBD/-}$ BMDMs (**Fig. 6E**). As expected, we did not observe any decay in the red tracker signal. Collectively, these data evidence that *Pik3ca*$^{RBD/-}$ BMDMs exhibit a significant impairment in removing engulfed particles, that can be attributed to the absence of lysosome acidification.

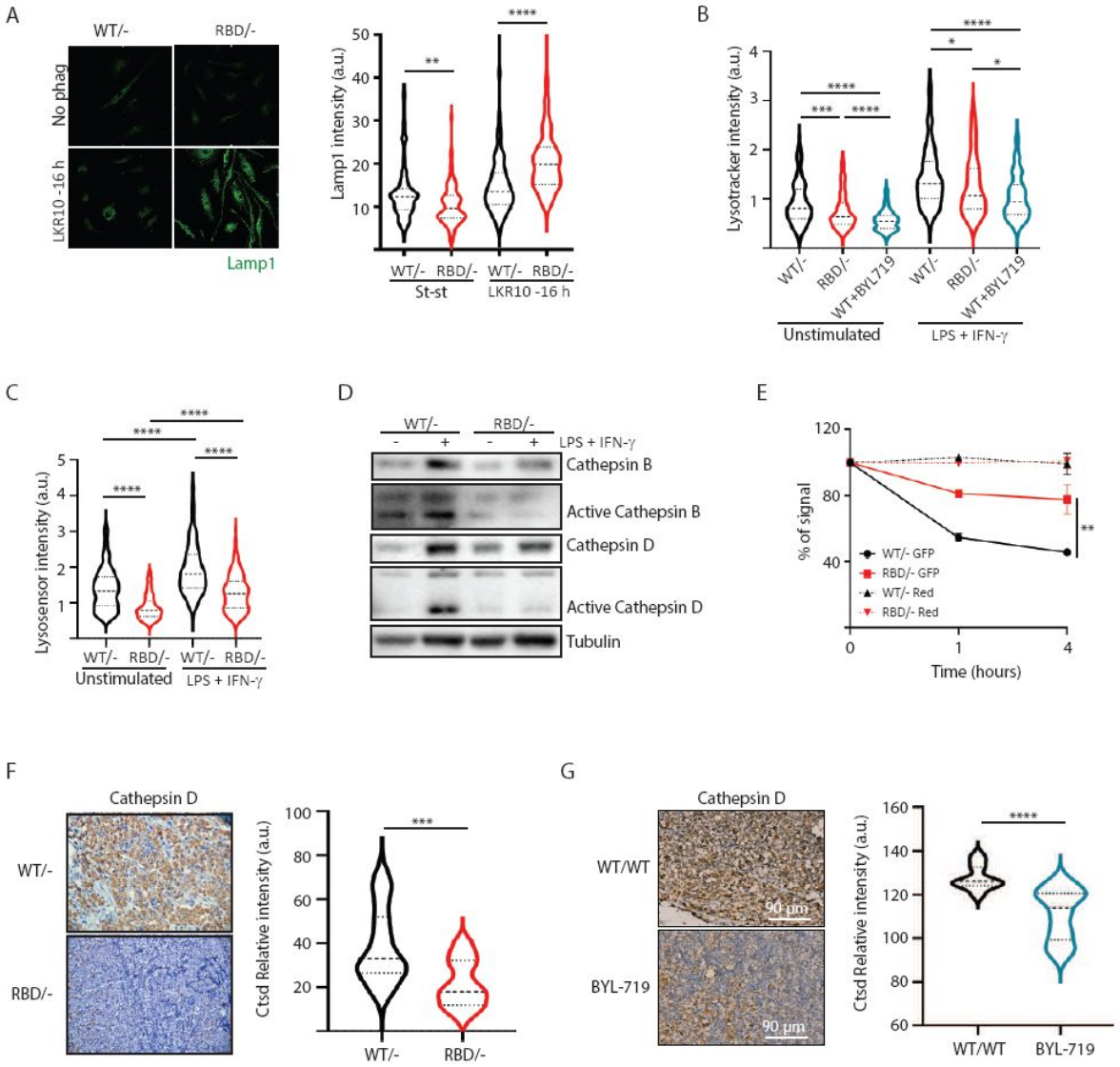

Figure 6.

Disruption of RAS-p110α activation in BMDMs leads to abnormal lysosomal function

(**A**) Representative IF images and quantification analysis of lamp intensity in *Pik3ca*$^{WT/-}$ and *Pik3ca*$^{RBD/-}$ BMDMs in steady state conditions and during phagocytosis of apoptotic LKR10 cells. Three independent biological replicates were analysed (n ≥ 250 total cells). Error bars indicate mean ± SEM; (**B**) Quantification analysis of lysosomal function in *Pik3ca*$^{WT/-}$, *Pik3ca*$^{RBD/-}$ and *Pik3ca*$^{WT/WT}$ BMDMs treated with BYL719 BMDMs unstimulated or activated with LPS + IFN-γ using Lysotracker staining. Three independent biological replicates were analysed (n ≥ 250 total cells); (**C**) Violin plot displaying lysosome pH acidity in unstimulated and LPS+IFN-γ stimulated *Pik3ca*$^{WT/-}$ (black), *Pik3ca*$^{RBD/-}$ (red) and *Pik3ca*$^{WT/WT}$ BMDMs treated with BYL719 (Blue) BMDMs, as determined by Lysosensor staining. Three independent biological replicates were analysed (n ≥ 250 total cells); (**D**) *Pik3ca*$^{WT/-}$ and *Pik3ca*$^{RBD/-}$ BMDMs were activated with LPS and IFN-γ and expression and activation of Cathepsin B and D were blotted; (**E**) Quantification of phagocytosed apoptotic cells in *Pik3ca*$^{WT/-}$, *Pik3ca*$^{RBD/-}$ and *Pik3ca*$^{WT/WT}$ BMDMs treated with BYL719 BMDMs. Apoptotic cells were labelled with a red tracker and allowed to be phagocytosed by control, *Pik3ca*$^{RBD/-}$ and *Pik3ca*$^{WT/WT}$ BMDMs treated with BYL719 for 16 hours, measuring the amount of cell tracker that was internalized at different time points. Each dot of the graph indicates a different independent experiment. Error bars indicate mean ± SEM; (**F**) Representative image and quantification of Cathepsin D expression in the inflammatory abscess of *Pik3ca*$^{WT/-}$ and *Pik3ca*$^{RBD/-}$ paws injected with zymosan; (**G**) Representative image and quantification of Cathepsin D expression in the inflammatory abscess of paws from control and *Pik3ca*$^{WT/WT}$ mice treated with BYL719 injected with zymosan.

Statistical significance was obtained using Mann-Whitney test: *p < 0.05; **p < 0.01; ***p < 0.001; ****p < 0.0001.

We have shown a delayed clearance of apoptotic cells in *Pik3ca*$^{RBD/-}$ mice after zymosan injection (**Fig. 1**). This, together with previous data took us to analyse the levels of Cathepsin D in the inflamed abscess from the paws of *Pik3ca*$^{RBD/-}$ and *Pik3ca*$^{WT/-}$ mice. Results showed a significant decrease in the levels of Cathepsin D in the inflamed area of *Pik3ca*$^{RBD/-}$ mice (**Fig. 6F**) and BYL719-treated mice (**Fig. 6G**).

Lysosomal digestion plays a pivotal role in activation of resolutive programs by mediating PPAR activation [50, 51]. Analysis of PPARδ and PPARγ expression in phagocyting macrophages showed a significant decrease in the expression of PPARδ, but no PPARγ in *Pik3ca*$^{RBD/-}$ BMDMs (**Supplementary Fig. S6A**), suggesting that resolutive programs might not be activated effectively.

In summary, our findings underscore the crucial role of RAS-p110α signalling axis in maintaining the balance of the inflammatory response and promoting timely resolution, providing further evidence for the significant involvement of RAS-p110α signalling in the response to inflammatory stimuli.

Discussion

In this study, we provide compelling evidence that disruption of RAS-p110α signalling or chemical inhibition of p110α impairs response to inflammatory stresses due to defects in both monocyte extravasation during the early stages of the inflammatory response and decreased lysosomal function during the later stages.

Monocyte extravasation during the inflammatory response is a critical step that allows immune cells to reach the site of infection or injury[19]. Impairment on this process causes slower or inadequate immune response, as macrophages are crucial for detecting and engulfing pathogens or cellular debris at the site of inflammation, as well as delayed resolution of inflammation, resulting in prolonged inflammation and potential tissue damage [52, 53]. Our data shows that RAS binding to p110α is involved in macrophage extravasation by modulating actin dynamics. During monocyte extravasation, actin filaments form actin-rich protrusions that are essential for monocyte migration across the endothelium[41, 54]. Our data show that, during extravasation, RAS-p110α signalling regulates actin dynamics so monocytes are able to squeeze through endothelial cells[41, 43].

The disruption of RAS-p110α in macrophages emerges as a pivotal determinant in cellular mechanics, elucidating a cascade of events resulting in increased F-actin levels. The increase in cytoskeletal components, particularly F-actin, causes a notable increase in cell stiffness and a concurrent decrease in cell deformability. The orchestration of these changes underscores the intricate balance in cytoskeletal dynamics. Notably, the regulatory role of Rho-GTPases comes into focus as potential mediators of this phenomenon. Rho-GTPases are well-known mediators of actin cytoskeletal rearrangements[55], and their dysregulation is known to impact cell mechanics[56, 57]. The observed increase in cell stiffness and deformability, may thus be governed by the modulation of Rho-GTPase activity. This intricate interplay provides a compelling avenue for further investigation into the molecular mechanisms through which RAS-p110α disruption influences Rho-GTPases, ultimately shaping the biomechanical properties of macrophages and may open avenues for therapeutic interventions targeting cytoskeletal dynamics in macrophages.

Monocyte extravasation shares many features with monocyte egression from the bone marrow. During monocyte egress, monocytes also undergo changes in cytoskeleton dynamics to detach from the sinusoidal endothelial cells and to migrate through the endothelial fenestrae and basement membrane into the bone marrow sinusoids[58]. Thus, the decrease in the number of

classical monocytes in the *Pik3ca*$^{RBD/-}$ mice in blood may be due, at least in part, to a defect in the extravasation process. This result may also explain, at least partially, the lack of macrophage recruitment to lung tumours found in previous studies using the RBD mouse model[11], [12].

Our findings also revealed a crucial role of RAS-p110α activation in the acute phase of the inflammatory response by regulating effective lysosomal degradation of phagocytosed and engulfed material. Phagocytosis constitutes a vital step in the inflammatory response, whereby phagosomes bind to lysosomes to form phagolysosomes in which pathogens are eradicated to facilitate an appropriate host response. This response encompasses antigen presentation to engage T-cell responses, secretion of inflammatory mediators that guide the adaptive immune response, and initiation of tissue repair mechanisms [22], [47]. Our data provide evidence that the activation of RAS-p110α signalling pathway is involved in the critical process of lysosomal acidification, which is essential for the efficient degradation of internalized particles and the activation of proteolytic enzymes, ultimately resulting in the formation of fully functional lysosomes. Consequently, lack of lysosome acidification impairs the expression and activation of important proteases such as cathepsin B and cathepsin D. The proper functioning of lysosomes is essential for mounting a robust response to inflammatory stress. Lysosomes play a central role in the breakdown of pathogens and dead cells by providing the necessary degradative enzymes and maintaining an acidic environment that facilitates the degradation of engulfed particles[20], [21]. When lysosomal function is compromised in macrophages, the degradation of phagocytosed material becomes impaired, leading to the accumulation of toxic debris. This accumulation subsequently triggers inflammation and causes damage to the surrounding tissues, leading to chronic inflammation and appearance of lysosomal storage diseases (LSD)[59], [60].

Our data showed that the disruption of Ras-p110α in macrophages presents a multifaceted impact in inflammatory response, notably manifesting as a reduction in NF-κB activation and cathepsin expression coupled with diminished lysosomal function. NF-κB, a pivotal regulator of inflammatory responses[61], [62], is intricately linked to lysosomal dynamics, with lysosomes playing a crucial role in modulating NF-κB signalling through the degradation of relevant molecules[63], [64]. Additionally, the observed decrease in NF-κB activation aligns with the decline in lysosomal function, which has previously been suggested in previous reports[65], [66]. This bidirectional influence, where perturbations in lysosomal function coincide with alterations in NF-κB activity, underscores the intricate and context-dependent nature of this regulatory network, suggesting a plausible mechanistic interdependence. Our data suggest that disruption in Ras-p110α signalling cascade could trigger downstream effects impacting both NF-κB activity and lysosomal integrity. This intricate nexus between Ras-p110α signalling, NF-κB activation, cathepsin expression, and lysosomal function underscores the complexity of cellular regulatory networks. Further analysis of the molecular pathways connecting these observations holds the potential to reveal novel insights into the coordinated regulation of inflammatory and lysosomal processes in macrophages. Thus, further investigations are necessary to decipher the causal relationships and unravel the broader implications of Ras-p110α disruption in shaping these intricate cellular responses during the inflammatory response.

The possible functional link between the increased actin polymerization and lysosomal dysfunction observed in *Pik3ca*$^{RBD/-}$ mice remains an unanswered question. Lysosome acidification and actin polymerization are tightly interconnected processes that have pivotal roles in numerous cellular functions[67]–[69]. Studies have demonstrated that lysosome acidification can influence actin polymerization dynamics through the activation of specific actin-binding proteins and the modulation of actin-regulatory proteins[67], [70]. Conversely, disruption in lysosome acidification, such as impaired proton pump activity or lysosomal storage disorders, have been associated with changes in actin polymerization and the organization of the cytoskeleton. Notably, it has been reported that depolimeryzation of F-actin plays a crucial role in assembling the macromolecular components of the acidification machinery in nascent endosomes[71]. Therefore, the intricate relationship between lysosome acidification and actin

polymerization suggests a potential reciprocal influence, where perturbations in one process could impact the other. Further investigation is required to determine the precise regulatory mechanisms by which p110α influences both lysosome acidification and actin polymerization, whether it occurs in a linear manner or through separate pathways.

This study provides valuable insights into the mechanisms that govern the immune response to inflammation, particularly emphasizing the essential role of RAS-p110α signaling. Our results underscore the pivotal role of RAS-p110α signaling in both the initiation and resolution of inflammation. The impaired ability of RAS-PI3K-deficient monocytes and macrophages to effectively migrate, initiate a robust inflammatory response, and resolve inflammation highlights the critical importance of this pathway in maintaining immune homeostasis. The persistent inflammation observed in these models may contribute to the development and perpetuation of chronic inflammatory conditions. Given the centrality of p110α in both initiating and resolving inflammation, its dysfunction could be a key factor in the chronic, dysregulated inflammation characteristic of diseases such as rheumatoid arthritis, inflammatory bowel disease, psoriasis, or systemic lupus erythematosus.

The potential of p110α as a therapeutic target in these conditions is especially intriguing. The recent identification of a p110α small molecule activator[72] offers a promising tool to explore this avenue. By transiently enhancing p110α function, it may be possible to promote the resolution of inflammation and thereby alleviate the symptoms and progression of these inflammatory diseases. Further research into this therapeutic strategy could open new pathways for treating chronic inflammatory disorders, providing much-needed relief for patients affected by these debilitating conditions.

Additional Declarations

The authors declare no competing interests.

Authors' Disclosures

The authors declare no conflict of interest.

Authors' Contributions

Conception and design: E. Castellano. **Development of methodology:** A. Rosell, M. Alcón Pérez, M.B. Voisin, J. de Paz, V. Rajeeve, C. Cuesta, O. Swinyard, E. Gabandé-Rodriguez, H. Fraile. **Acquisition of data (provided animals, acquired and managed patients, provided facilities, etc.):** A. Rosell, M. Alcón Pérez, A. Krywoska, M.B. Voisin, J. Downward, P. Cutillas, C. García-Macías, J. Alcaraz, E. Castellano. **Analysis and interpretation of data (e.g., statistical analysis, biostatistics, computational analysis):** A. Rosell, M. Alcón Pérez, A. Krywoska, M.B. Voisin, V. Rajeeve, A. Berral-Gonzalez, J. De Las Rivas, P. Cutillas, E. Castellano. **Writing, review, and/or revision of the manuscript:** A. Rosell, M. Alcón Pérez, M.B. Voisin, J. De Las Rivas, P. Cutillas, E. Castellano.

Acknowledgements

This work was supported by grants from the Spanish Ministry of Science and Innovation (RTI2018-099161-A-I00), Programa JAE-Intro ICU from CSIC (JAEICU-21-IBMCC-6), JCyL (CSI185-20), Marie Curie Initial Training Network on Tumour Infiltrating Myeloid Cell Compartment (PF7 MCA-ITN317445) and CRUK-Barts Cancer Centre Development Fund. This research was co-financed by FEDER funds. The CIC is supported by the Programa de Apoyo a Planes Estratégicos de Investigación de Estructuras de Investigación de Excelencia of Castilla y León autonomous government (CLC-2017-01) and AECC Excellence program Stop Ras Cancers (EPAEC222641CICS). The authors wish to thank the Pathology Unit, the Mouse Model Experimentation Unit, and the Advanced Cellular Analysis Unit at CIC for their assistance in carrying out this work.

Methods

Animal studies

For removal of Pik3ca-floxed allele, Pik3ca$^{RBD/lox}$ and Pik3ca$^{WT/flox}$ mice[64] were given 3.2 mg tamoxifen (Sigma) dissolved in 80 µl of corn oil by oral gavage once per day during 3 consecutive days. Efficiency of tamoxifen treatment was routinely performed by genotyping for the presence of the floxed allele.

For ***paw oedema studies*** *Pik3ca$^{RBD/-}$* and *Pik3ca$^{WT/-}$* mice[64] were divided into groups of four two weeks before oedema induction. Before inducing the paw oedema, the mice were anesthetized with 4% isofluorane. To induce the oedema, mice received ipsilateral i.pl. injection (30 µl) of either zymosan (10 µg/µl, Sigma Aldrich) or PBS into the back-hind paw. Injection of 0.1mg/kg Buprenorphine (NOAH, Vetergesic) was given for pain prevention. Paw thickness was measured using a calliper every hour during the first 6 hours after injection and then at 8, 10 hours and twice per day afterwards. Buprenorphine was injected twice per day during the length of the experiment. Mice were kept, managed, and sacrificed in the NUCLEUS animal facility of the University of Salamanca according to current European (2007/526/CE) and Spanish (RD 1201/2005 and RD53/2013) legislation. All experiments were approved by the Bioethics Committee of the Cancer Research Center.

Isolation, culture and treatments of BMDM

Bone marrow cells from tibias and femurs of 12–14-week-old Pik3ca$^{RBD/Lox}$ mice and Pik3ca$^{WT/Lox}$ littermates were cultured with DMEM supplemented with 10% FBS, 100 units/ml penicillin, 100 µg/mL streptomycin, 2 mM L-Glutamine and 20 ng/mL M-CSF for 7 days. 4-hydroxytamoxifen (Sigma Aldrich) (100 nM) was added to culture media on day 3 to eliminate *Pik3ca*-Lox allele. The differentiated BMDM were then detached using cell dissociation buffer (C5914-100, Merck) and cultured in DMEM supplemented with 10% FBS, 100 µg/mL streptomycin, 2 mM L-Glutamine, 20 ng/mL M-CSF for unstimulated BMDMs. For macrophage polarization towards an inflammatory phenotype 20 ng/ml IFNγ (Peprotech) and 100 ng/ml LPS (Sigma Aldrich) was added to culture media.

Generation of chimeric animals

Chimeric mice exhibiting WT or RBD deficient leukocytes were generated by lethal irradiation with 5.5 Gy twice, 4 h apart of LysM GFP recipient animals (mice exhibiting endogenously GFP fluorescent monocytes and neutrophils) followed by an injection of bone marrow cells (1.5×10^6

cells/recipient i.v.) from C57BL/6 WT or RBD donor mice. Chimerism was then assessed 4 weeks later by flow cytometry from blood samples (reconstitution of 99.8 ± 0.2 % and 99.8 ± 0.1% for WT and RBD deficient donor cells, respectively; n =5 mice per group).

Neutrophil depletion

Neutrophil depletion of chimeric mice was induced by intraperitoneal injection of anti-GR1 25µg/mouse/day for 3 days). Numbers of blood circulating monocytes and neutrophils were quantified by flow cytometry pre- and post-depletion. Neutrophils were found to be reduced by 99.5%, whilst this anti GR1-depleting protocol had no effect on blood monocyte proportion (n=5 mice/group).

Brightfield intravital confocal microscopy

Mesenteric inflammation was induced following intraperitoneal injection of mouse recombinant CCL2 (500ng/mouse in 500uL of PBS). Six hours later, anesthetized chimeric mice (150 mg/kg ketamine, 7.5 mg/kg xylazine, i.p.) were placed in supine position on a heating pad (37 °C) for maintenance of body temperature. The mesenteric vascular bed was exteriorized, placed on a purpose-built stage of an upright brightfield microscope (Zeiss Axioskop). Mesenteries were superfused with warmed (37 °C) Tyrode's solution (Sigma). After a 5-min equilibration period, analysis of leukocyte-endothelium interactions was made in at least 9 (and up to 16) randomly selected segments (100 µm in length) of post-capillary venules (20–40 µm in diameter) for each mouse. Leukocyte rolling was quantified by counting the number of rolling cells passing a fixed transversal line in the middle of the vessel segment for 5 min. Leukocyte adhesion (stationary position of the cell for 30 s or longer) was quantified along a 100 µm vessel length and data were normalized as the number of cells per 500um vessel segments. Leukocyte extravasation response was quantified within 50 µm on either side of the 100 µm vessel segment in the perivenular tissue; and data were normalized as the number of extravasated leukocytes per mm2 of extravascular tissue. At the end of the analysis period, mice were humanely killed by cervical dislocation.

BMDM elastic modulus

The elastic modulus of BMDMs was quantitatively assessed utilizing Atomic Force Microscopy (AFM). Specifically, cells were cultured on cover glass slides, which were subsequently positioned in a specialized BIO-AFM setup integrated with an inverted optical microscope (Nikon TE2000). The BIO-AFM was equipped with a V-shaped, four-sided pyramidal silicon nitride tip (Bruker AFM Probes) to facilitate accurate force measurements. To avoid localized variations and ensure data representativeness, no more than three cells were selected from a single field of view for mechanical characterization, and these cells were never contiguous. Subsequently, the stiffness of each individual cell was characterized through measurements obtained at three perinuclear points. For each point, force-displacement (F vs. z) curves were captured (10 µm amplitude at a speed of 5 µm/s). The determination of the elastic modulus was performed based on the analysis of force-displacement curves. A total of five curves were recorded for each perinuclear point at an indentation depth of 300 nm. Data were analysed by fitting the curves to the Hertz model as previously described[73,74]. Finally, the elastic modulus for each cellular population under distinct experimental conditions was calculated based on a minimum of fifteen measurements per independent cell, with each condition comprising at least ten independent cells (n ≥ 10).

Cytokine arrays

Bone marrow-derived macrophages (BMDMs) were cultured in 6-well plates at a density of 1×10^6 cells per well. Cytokine production was analyzed in unstimulated and M1 macrophages using commercial mouse cytokine array (R&D Systems, #ARY006). Cells were lysed at 4°C for 30 minutes using a lysis buffer containing 1% Igepal CA-630, 20mM Tris-HCl (pH 8.0), 137mM NaCl, 10% glycerol, 2mM EDTA, 10µg/ml Aprotinin, 10µg/ml Leupeptin, and 10µg/ml Pepstatin, following the manufacturer's protocol. Lysates were then centrifuged at 16,100 RCF for 15 minutes at 4°C. The

supernatant was collected, and protein concentration was determined using a Qbit 2.0 Fluorometer. A total of 1400µg of protein was diluted to a final volume of 1ml with Array Buffer 6, followed by the addition of 0.5ml Array Buffer 4 and 15µl of the reconstituted Mouse Cytokine Array Panel A Detection Antibody Cocktail. The samples were mixed and incubated for one hour on a shaker at room temperature. Nitrocellulose membranes from the mouse cytokine array were blocked with Array Buffer 6 for one hour at room temperature on a shaker. The blocking buffer was then removed, and the sample mixture was added to the arrays, which were incubated overnight at 4°C on a shaker. Membranes were washed with Wash Buffer provided by the manufacturer. Membranes were then incubated with 1× Streptavidin-HRP in Array Buffer 6 for 30 minutes at room temperature. After further washing, the Chemi Reagent Mix was applied, and signals were detected using an Amersham Imager 600 (GE Healthcare, #29-0981-07 AC).

Immunofluorescence

BMDM were fixed using 4% paraformaldehyde, permeabilized with 0.1% Triton X-100 and blocked for 1 h with 3% BSA in PBS before incubation with the primary antibodies, used at a 1:100 dilution: Lamp1 (#553792, BdPharmigen), Deoxyribonuclease I-Alexa Fluor™ 488 Conjugate (#D12371, Invitrogen, 1:2000). To stain actin cytoskeleton, Alexa Fluor™ 647 Phalloidin (Invitrogen, 1:10 000) was directly added to the primary antibody mixture. Alexa Fluor 488- or Alexa Fluor 555-conjugated secondary antibodies (Invitrogen) were used to detect the indicated proteins at a 1:1000 dilution. Cells were counterstained with DAPI on the mounting solution (ProLong Gold Antifade Reagent with DAPI, Invitrogen). Images were taken using a Zeiss LSM510 confocal microscope or Leica DM6 B THUNDER Imager 3D Tissue.

Transwell migration assay

Transwell migration assays were carried out using the 6.5 mm Transwell® with 8.0 µm Pore Polyester Membrane Insert (Corning). 9×10^4 MEFs from wild type mice were used as a chemo-attractant to encourage macrophage migration. 8×10^5 BMDM were seeded in the transwell. Transwells were performed following the manufacturer instructions.

Random migration assay

For random migration assays, BMDMs were seeded in 24-well plates coated with matrigel (0.5mg/ml) and labelled using CellTracker™ Red CMTPX Dye 1 µM (ThermoFisher) for 30 minutes. 24 hours later LPS + IFN-γ was added when necessary. Triplicates of each condition and genotype were prepared. Time-lapse imaging was carried out for 24 h. One image was taken every 10 min within the same well using a Nikon microscope driven by Metamorph (Molecular Devices, Chicago, IL, USA). A total of 80–100 cells per condition were tracked using the Fiji plugin Trackmate. Pre-processing was done using Mexican hat filter 3.0 radius to increase particle detection. Images were segmented using the fluorescence channel with the Laplacian of the Gaussian detector with a 30 µm estimated particle diameter, a 10.0 threshold and median filter option selected. Segmented objects were linked from frame to frame with a Linear Assigment Problem (LAP) tracker with 45 µm frame-to-frame linking distance and 2 frame gap closure. Criteria for track acceptance were track duration at least the 90% of the video. Tracks were visually inspected for completeness and accuracy of the tracking.

Secretome mass spectrometry

Samples for secretome analysis were prepared as previously described[130]. In brief, 100ug of proteins were digested into peptides using trypsin and peptides were desalted using Oasis HLB extraction cartridges (Waters UK Ltd)) and eluted with 50% acetonitrile (ACN) in 0.1% Trifluoroacetic acid (TFA).

Dried peptides were dissolved in 0.1% TFA and analysed by nano ACQUITY liquid chromatography (Waters Corp., Milford, MA, USA) coupled on-line to a tandem LTQ Orbitrap XL, mass spectrometer (Thermo Fisher Scientific)[131]. Gradient elution was from 5% to 25% buffer B in 180 min at a flow rate 300nL/min with buffer A being used to balance the mobile phase (buffer A was 0.1% formic acid in water and B was 0.1% formic acid in ACN). The mass spectrometer was controlled by Xcalibur software and operated in the positive mode. The spray voltage was 1.95 kV and the capillary temperature was set to 200 °C. The LTQ Orbitrap XL was operated in data dependent mode with one survey MS scan followed by 5 MS/MS scans. Label-free quantitative proteomics analysis was performed using three independent biological samples per group. Additionally, each sample was analysed in technical duplicates. To ensure robust quantitative analysis, we utilized LTQ Orbitrap XL tandem mass spectrometry (MS/MS) to generate six distinct mass spectral profiles from each group.

MS raw files were converted into Mascot Generic Format using Mascot Distiller (version 2.3.0) and searched against the SwissProt database (release December 2015) restricted to human entries using the Mascot search daemon (version 2.3.1). Allowed mass windows were 10 ppm and 600 mmu for parent and fragment mass to charge values, respectively. Variable modifications included in searches were oxidation of methionine, pyro-glu (N-term) and phosphorylation of serine, threonine and tyrosine.

Spectral counting quantification method relies on the number of times peptides are identified by tandem mass spectrometry (with expectancy value <0.05) from a given protein. Spectral counts were obtained from Mascot result (DAT) files using a python script written in house in the Mascot Parser Toolkit environment (version 2.4.x).

Proteomic data analysis

The proteomic data obtained consisted of 6,844 peptides and 30 samples: Pik3ca$^{WT/-}$ and Pik3ca$^{RBD/-}$ BMDMs in steady state conditions (labelled as cell samples: WT/- and RBD/-), phagocytosing apoptotic cells (labelled as cell samples: WT/-Phag and RBD/-Phag), and the apoptotic LKR10 cells alone (labelled as LKR). For each of these samples, proteomic experiments were performed with 6 replicates (3 biological replicates × 2 technical replicates), yielding a data set of 30 samples.

The first analytical step was to remove all peptides for which there was no information contained in the proteomic raw data matrix and the peptides for which 85% or more of the signal values were missing. All these peptides were specific of mouse proteins and in many cases were unique. The corresponding proteins were annotated and labelled together with each measured peptide. Next, low-quality samples were also removed, testing the overall signal per sample to identify if there were clear outliers with very low signal or with a very different signal distribution. Comparison of the overall signal distributions of the 30 samples (comparing boxplots) and identified 3 samples that were very different were obtained and discarded (WT/-Phag_s3r2 (sample 3, replicate 2), RBD/-_s2r1 and LKRc_s1r1). These 3 samples showed a median signal in their distributions that deviated >20% from the median signal of the distributions of all other samples.

Differential expression analysis for each peptide of each protein were next performed. The algorithm used to carry out this analysis was *limmaVoom* within EdgeR R package[75, 76]. Prior to this analysis, a Bartlett test was performed to see the homogeneity of variances, verifying that for this data we cannot consider equality of variances and this factor was included in the differential expression algorithm. With this algorithm, normalization factors to use *a-posteriori* were calculated and, transformation and calculation of the variance weights was performed. The model to fit before using *Voom* as specified since it uses the variances of the model's residuals (observed - fitted). Finally, an estimation of the contrast for each feature tested (i.e. each peptide) was carried out using the *Empirical Bayes* approach in *limma* as previously described[77].

Peptides were ordered by the p.value of the *limma* test considering significant peptides changed only with a p.value below 0.05 and with a log2(Fold-Change) >|2|. All these analyses were performed using the statistical computing language R and packages or libraries obtained from R-cran (cran.r-project.org) or Bioconductor (*www.bioconductor.org*).

Cytoscape software (v3.9)[78] including GeneMania app[79] was then used to generate and visualize protein-protein networks of the significantly altered proteins selected in secretome analysis of unstimulated and phagocyting BMDMs. This tool provides information on protein-protein associations based in co-expression studies and also based in physical interaction studies.

Western blot analysis

Immunoblot was performed per a general western-blot protocol (Abcam). Total protein was extracted using Cell Lysis Buffer (Cell Signaling Technology) supplemented with c0mplete mini protease inhibitor cocktail (Roche), 50 mM sodium fluoride and 1 mM of PMSF. Protein was quantified using Bradford Method (Bio-Rad). 20 µg of protein was separated by SDS-PAGE and transferred to 0.2 um pore-size PVDF membranes (Sigma-Aldrich). Blots were probed using the following antibodies, at a concentration 1:1000 unless otherwise stated: cathepsin B (12216-1-AP, Proteintech), cathepsin D (21327-1-AP, Proteintech), α-tubulin (ab15246, Abcam; concentration 1:5000). Horseradish peroxidase-conjugated secondary antibodies (Amersham) were used (1:5000) and detected using an enhanced chemiluminescent substrate (Amersham). Signal was detected using an iBright 1500 System (Invitrogen).

Flow cytometry analysis

Single-cell suspensions from cultured cell, spleen or blood monocytes were generated from mice, washed twice in staining buffer and incubated with 1:100 Fc-block (BD Biosciences, #553142) diluted in FACS buffer. Cells were subjected to surface antibody staining with labelled antibodies diluted in staining buffer for 30 min at 4 °C: CD3-PE-Cy7 (#100328, Biolegend), CD4-BV605 (#100548, Biolegend), CD8-APC (#100712, Biolegend), CD19-PerCP-Cy5.5 (#115534, Biolegend), CD45-BV785 (#103149, Biolegend), Ly6C-PerCP-Cy5.5 (#128012, Biolegend), Ly6C-E450 (#48-5932-82, eBioscience), Ly6G-AF700 (#56-5931-82, eBioscience), CD11b-BV650 (#101239, Biolegend), F4/80-PE-Cy7 (#123114, Biolegend), F4/80-PE (#123110, Biolegend), CCR2 (CD192)-PE-Vio ® 770 (#130-108-724, Miltenyi Biotec). After incubation, cells were washed in staining buffer and analysed immediately. For all staining, isotype controls were used.

The gating strategy for analysing distinct cellular populations began by isolating cells positive for the CD45 marker. Subsequently, B cells, identified by their positivity for CD19 and negativity for CD11b, were selected. To determine the frequency of T cells, the CD45+ cell population, devoid of both CD19 and CD11b, underwent examination for CD3 expression. CD3+ cells were further categorized based on CD4 and CD8 expression, distinguishing CD4+, CD8+, and double-negative (DN) T cells. Following the application of these gating criteria across all samples, the percentages of CD45-positive cells expressing CD19 and T cells (CD3+) within the CD45+ population were calculated. Additionally, myeloid populations were analysed by quantifying the proportion of CD11b+ cells. To distinguish between circulating monocytes and granulocytes, we assessed their expression of Ly6G (granulocytes) and Ly6C proteins (monocytes). Classical monocytes were characterized by negativity for Ly6G and positivity for Ly6C, while alternative monocytes lacked both markers, and neutrophils/granulocytes displayed weak positivity for Ly6C and positivity for Ly6G.

Samples were acquired on a BD LSR FORTESA FACS or FACS Aria III machine that uses FACS DIVA software (BD Biosciences). Compensation was performed using 1 drop of Ultracomp ebeads (eBioscience) in 300αl of FACS buffer. 1µl of each antibody used in the pool was mixed with 100µl

of compensation beads solution and acquired. A total of 50000 cells per mouse were analysed. Analysis was performed with FlowJo software (FlowJo V10.4). Once the different pools were compensated samples were acquired.

Phagocytosis assay

For phagocytosis assay, BMDMs in suspension in DMEM without FBS were labelled with 1:200 red cell tracker (Molecular Probes) for 30 minutes at 37°C. Cells were then centrifuged for 5 minutes at 300g at 4°C, supernatant was removed and labelled BMDMs were washed twice with 5ml of PBS and plated overnight in complete DMEM containing 20 ng/ml M-CSF. On the following day, 100 ng/ml LPS (Sigma Aldrich) was added to BMDMs overnight.

LKR10 cells (murine lung cancer cell line) were stained with red cell tracker (Molecular Probes) as previously described for macrophages. Stained cells were plated in complete DMEM medium and, after 12 hours, 50 µM Cisplatin (MCE MedChemExpress) was added to the media and left overnight. BMDMs were then incubated with apoptotic cancer cells at a 1:2 ratio and cultured at 37 °C for different time points in DMEM supplemented with 10% FBS.

Flow cytometry data were acquired using a BD LSR FORTESSA FACS instrument with FACS DIVA software (BD Biosciences) and analysed using FlowJo V10.4 software. A minimum of 2×10^5 events were acquired and analysed. Data analysis and interpretation was done using FlowJo software (FlowJo V10.4).

Image analysis

Confocal images were post-processed and analysed using Fiji distribution of ImageJ version 1.53q. Cell shape descriptors such as “aspect ratio” (AR), “circularity” (C) and “cell area” were measured using Fiji. Specifically, aspect ratio is calculated as (major axisxminor axis-1) therefore representing solely the degree of elongation, whereas circularity is calculated as [4π*(area × perimeter-2)], thus representing the degree of similarity to a circumference with a value ranging from 0 to 1 (perfect circle).

Histology

Tissue was fixed using 4% formaldehyde for 48h, dehydrated and paraffin-embedded. Sections (3 µm) were cut and stained using hematoxylin-eosin. For immunodetection, citrate pH 6 buffer was used for antigen retrieval. Staining was used using the following primary antibodies: CD68 (ab125212, Abcam, 1:200), cathepsin B (12216-1-AP, Proteintech, 1:100), cathepsin D (21327-1-AP, Proteintech, 1:400). Dako EnVision+ System HRP labelled Polymer secondary antibodies (Dako) were used, and DAB+ Substrate Chromogen System (Dako) was used for color development.

For the quantification of loose chromatin remnants in paw edema images, the pathologist assigned a score ranging from 1 to 3 based on the chromatin content within the inflammatory abscess. A score of 1 indicates low chromatin content, occupying less than 30% of the abscess area, while a score of 3 represents high chromatin content, covering over 60% of the abscess area.

Supplementary Data

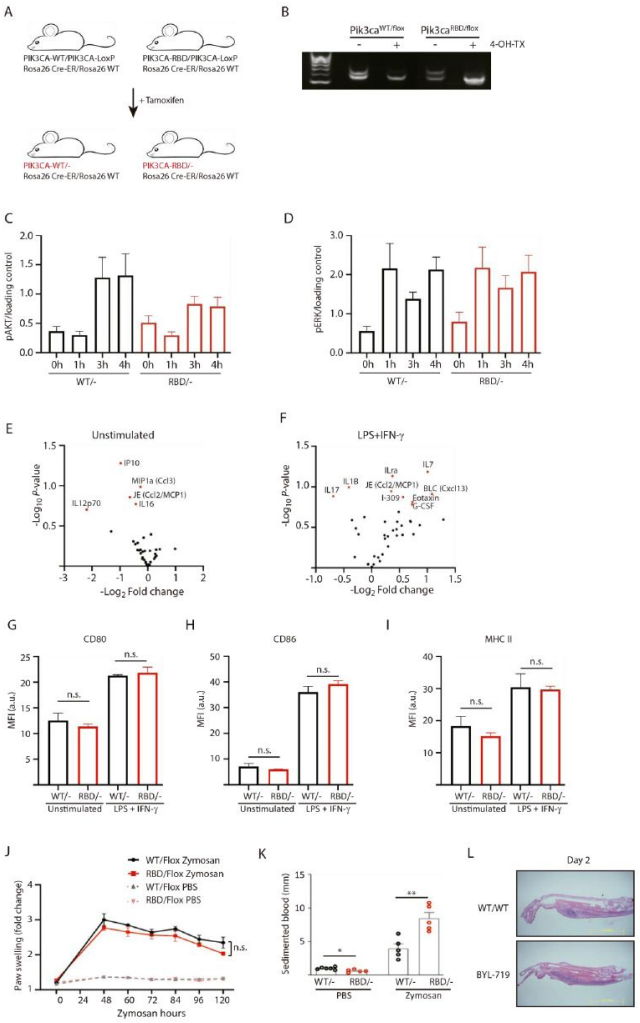

Supplementary Figure S1.

Pik3ca$^{RBD/-}$ mice have more extended inflamed tissue after zymosan injection

(A) Schematic representation of the mouse model used in which the interaction of p110α with RAS was disrupted by the introduction of two-point mutations, T208D and K227A, into the endogenous Pik3ca gene (*Pik3ca*^{RBD}). Wild-type (*Pik3ca*^{WT}) and *Pik3ca*^{RBD} mice were bred with mice containing a floxed *Pik3ca* allele and a mouse carrying a conditional Cre recombinase (Cre-ERT2) allele targeted to the ubiquitously expressed Rosa26 locus; **(B)** Representative PCR showing efficiency of floxed allele removal after treatment with 4-hydroxytamoxifen for 48 hours; **(C)** Graph quantifying p-AKT signal from 3 independent WB and normalized against its loading control; **(D)** Graph quantifying p-ERK signal from 3 independent WB and normalized against its loading control; **(E)** Volcano plots corresponding to identified cytokines differentially expressed in unstimulated BMDMs; **(F)** Volcano plots corresponding to identified cytokines differentially expressed in LPS + IFN-γ BMDMs; **(G) (H) (I)** Pik3caRBD/- and Pik3caRBD/- BMDMs were stimulated with LPS+IFN? and expression of (G) CD80; (H) CD86; and (I) MHCII were analysed by flow cytometry (Pik3caRBD/- n = 5; Pik3caWT/- n = 3). Error bars indicate mean ± SEM. Significance using Mann-Whitney test: n.s. no-significant.; **(J)** Pik3ca$^{WT/Flox}$ and Pik3ca$^{RBD/Flox}$ mice were injected with zymosan or PBS in the back-hind paws and inflammation was measured and plotted over time, Pik3ca$^{WT/Flox}$ n = 5; Pik3ca$^{RBD/Flox}$ PBS n = 5; Pik3ca$^{WT/Flox}$ Zymosan n = 5; Pik3ca$^{RBD/Flox}$ Zymosan n = 5; Error bars indicate mean ± SEM. Significance using 2-way ANOVA test: n.s. non-significant **(K)** Blood from the same mice was obtained by cardiac puncture prior culling and blood sedimentation was measured. The clear layer formed at the top was used for data quantification. Black dots represent data from *Pik3ca*$^{WT/-}$ mice and red dots represent data from *Pik3ca*$^{RBD/-}$ mice. Each dot represents an individual mouse. Each dot represents an individual mouse. Error bars indicate mean ± SEM. Significance using Student's t test: * p < 0.05; **p < 0.01. *Pik3ca*$^{WT/-}$ PBS n = 6; *Pik3ca*$^{RBD/-}$ PBS n = 5; *Pik3ca*$^{WT/-}$Zymosan n = 4; *Pik3ca*$^{RBD/-}$ Zymosan n = 4; **(L)** Representative images showing zymosan-induced inflammatory area in *Pik3ca*$^{WT/WT}$ mice and *Pik3ca*$^{WT/WT}$ mice treated with BYL-719.

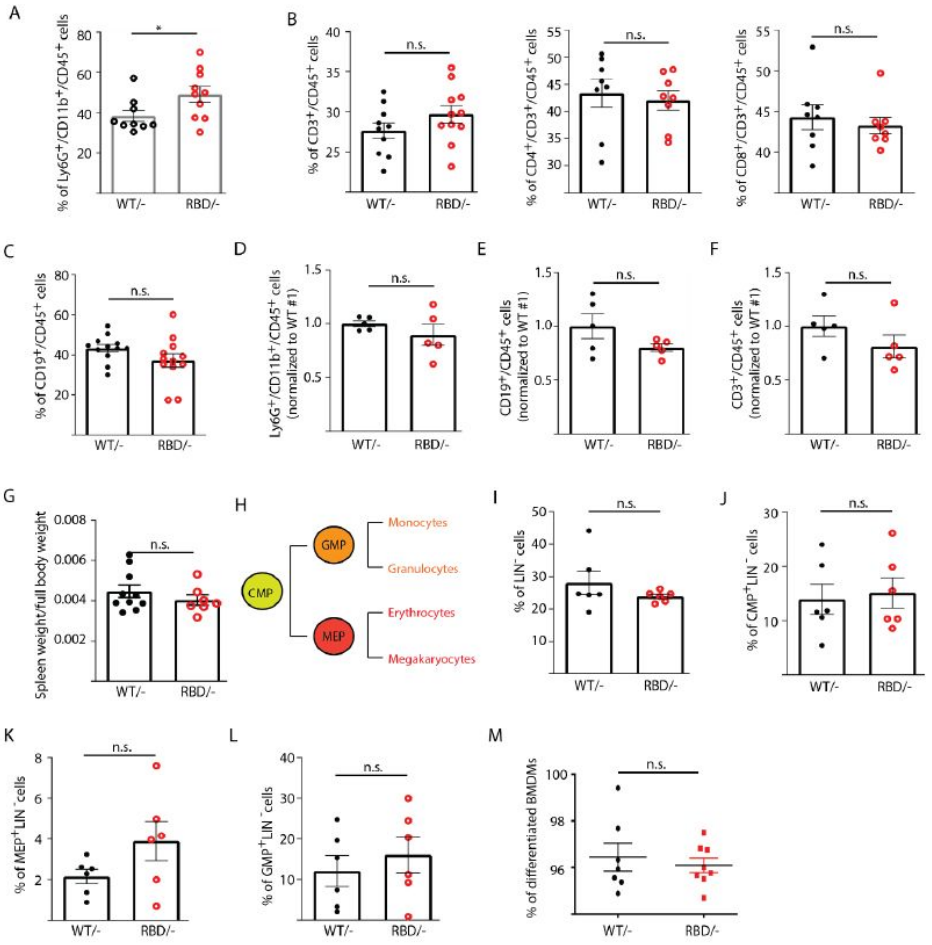

Supplementary Figure S2.

Disruption of RAS-p110α interaction does not affect the number of B-cells or T-cells in blood or spleen.

Twelve-week-old mice were treated with tamoxifen and after four weeks, flow cytometry analysis was performed to determine abundancy of different immune populations. **(A)** Granulocytes in circulating blood; **(B)** CD3, CD4+ and CD8+ T-cells in circulating blood; **(C)** B-cells in circulating blood; **(D)** Granulocytes in spleen; **(E)** B-cells in spleen; **(F)** T-cells in spleen; **(G)** Spleen weight compared to full body; **(H)** Schematic representation of myeloid precursors differentiation (CMP-common myeloid progenitor; GMP-Granulocyte-monocyte progenitor; MEP-Megakaryocyte-erythroid progenitor); **(I)** Graph showing percentage of bone marrow cells progenitor cells (have not acquire any lineage marker, Lin^-); **(J)** Graph showing percentage of CMP cells within progenitor cells; **(K)** Graph showing percentage of MEP cells within progenitor cells; **(L)** Graph showing percentage of GMP cells within progenitor cells; **(M)** Graph depicting % of differentiated macrophages obtained in culture from bone marrow precursors in the presence of m-CSF. Black dots represent data from *Pik3ca*$^{WT/-}$ mice and red dots represent data from *pik3ca*$^{RBD/-}$ mice. Each dot represents an individual mouse. Error bars indicate mean ± SEM. Significance using Student's t test: n.s. non-significant.

Supplementary Figure S3.

Pik3ca$^{RBD/-}$ monocytes do not extravasate through the endothelium.

(A) Graph showing levels of neutrophil reconstitution in chimera's bone marrow. Blood from chimera mice was collected and GFP in granulocytes was analysed by flow cytometry to determine engraftment percentage. (**B**) Graph quantifying the number of monocytes in the blood of chimera mice treated with anti-GR1 (25µg/mouse/day) for 3 days. **(C)** Graph showing levels of expression of CCR2 in *Pik3ca*$^{WT/-}$ and *Pik3ca*$^{RBD/-}$ BMDMs detected by flow cytometry. Error bars indicate mean ± SEM. Significance using Mann-Whitney test: n.s. no-significant

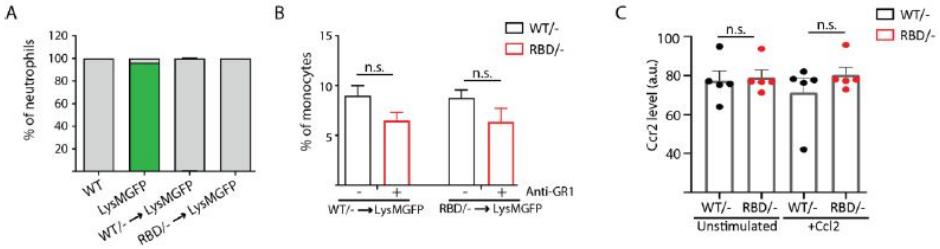

Supplementary Figure S4.

Disruption of RAS-p110α interaction has a differential role in phagocytosis.

(A) Graph representing the ability of *Pik3ca*$^{RBD/-}$ and *Pik3ca*$^{RBD/-}$ BMDMs to phagocyte sepharose beads. Data from 3 independent experiments are presented; **(B)** Graph representing the ability of *Pik3ca*$^{RBD/-}$ and *Pik3ca*$^{RBD/-}$ BMDMs to phagocyte *Borrelia burgdorferi*. Data from 6 independent mice are presented. Error bars indicate mean ± SEM. Significance using Mann-Whitney test: * p < 0.05; **p < 0.01; n.s. no-significant

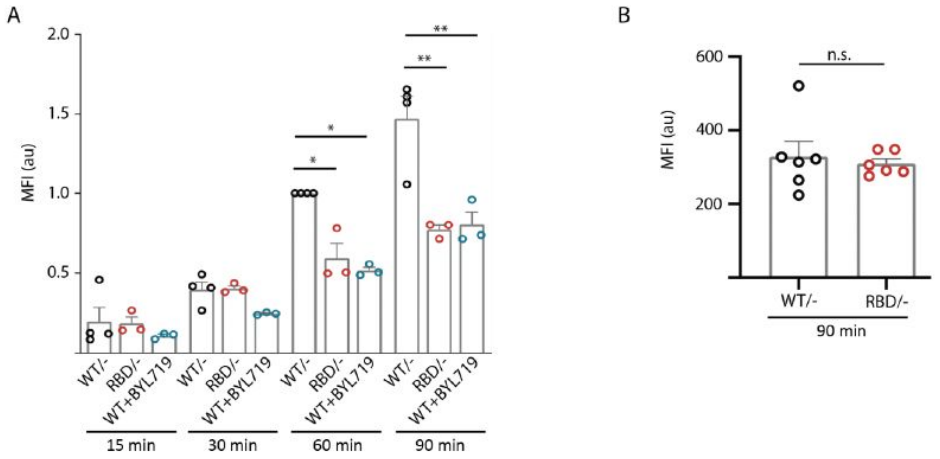

Supplementary Figure S5.

Disruption of RAS-p110α interaction alters the secretome of BMDMs.

(A) WB showing induction of apoptosis in LKR10 cell line treated with cisplatin for 16 hours; **(B)** Dendrogram showing hierarchical clustering of peptides found in the secretome analysis of *Pik3ca*$^{RBD/-}$ and *Pik3ca*$^{RBD/-}$ BMDMs in steady state conditions; **(C)** Dendrogram showing hierarchical clustering of peptides found in the secretome analysis of *Pik3ca*$^{RBD/-}$ and *Pik3ca*$^{RBD/-}$ BMDMs phagocytosing apoptotic cells.

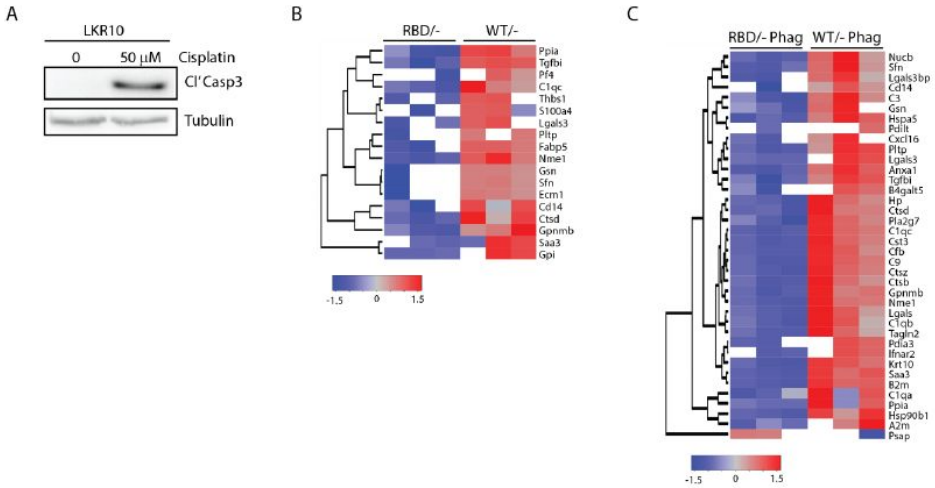

Supplementary Figure S6.

Disruption of RAS-p110α interaction impacts expression of inflammation resolution mediators.

Pik3ca$^{RBD/-}$ and *Pik3ca*$^{RBD/-}$ BMDMs were set up to phagocyte apoptotic cells and expression of **(A)**Pparδ and **(B)** Ppary was measured by qPCR.

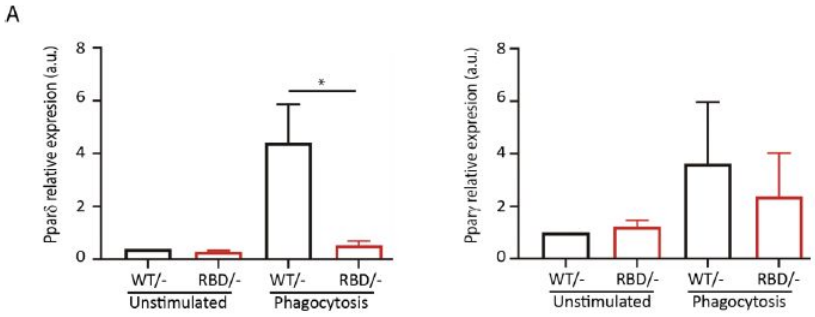

References

1. Cuesta C., Arevalo-Alameda C., Castellano E. (2021) **The Importance of Being PI3K in the RAS Signaling Network** *Genes (Basel)* **12**

2. Cantley L.C. (2002) **The phosphoinositide 3-kinase pathway** *Science* **296**:1655–1657

3. Castellano E., Downward J. (2011) **RAS Interaction with PI3K: More Than Just Another Effector Pathway** *Genes Cancer* **2**:261–274

4. Madsen R.R., Vanhaesebroeck B. (2020) **Cracking the context-specific PI3K signaling code** *Sci Signal* **13**

5. Troutman T.D., Bazan J.F., Pasare C. (2012) **Toll-like receptors, signaling adapters and regulation of the pro-inflammatory response by PI3K** *Cell Cycle* **11**:3559–3567

6. Vergadi E., Ieronymaki E., Lyroni K., Vaporidi K., Tsatsanis C. (2017) **Akt Signaling Pathway in Macrophage Activation and M1/M2 Polarization** *J Immunol* **198**:1006–1014

7. Kok K., Geering B., Vanhaesebroeck B. (2009) **Regulation of phosphoinositide 3-kinase expression in health and disease** *Trends Biochem Sci* **34**:115–127

8. Hawkins P.T., Stephens L.R. (2015) **PI3K signalling in inflammation** *Biochim Biophys Acta* **1851**:882–897

9. Okkenhaug K. (2013) **Signaling by the phosphoinositide 3-kinase family in immune cells** *Annu Rev Immunol* **31**:675–704

10. Tamura N., et al. (2009) **Specific role of phosphoinositide 3-kinase p110alpha in the regulation of phagocytosis and pinocytosis in macrophages** *Biochem J* **423**:99–108

11. Castellano E., et al. (2013) **Requirement for interaction of PI3-kinase p110alpha with RAS in lung tumor maintenance** *Cancer Cell* **24**:617–630

12. Murillo M.M., et al. (2014) **RAS interaction with PI3K p110alpha is required for tumor-induced angiogenesis** *J Clin Invest* **124**:3601–3611

13. Bennett J.M., Reeves G., Billman G.E., Sturmberg J.P. (2018) **Inflammation-Nature's Way to Efficiently Respond to All Types of Challenges: Implications for Understanding and Managing "the Epidemic" of Chronic Diseases** *Front Med (Lausanne)* **5**

14. Chaplin D.D. (2010) **Overview of the immune response** *J Allergy Clin Immunol* **125**:S3–23

15. Chen L., et al. (2018) **Inflammatory responses and inflammation-associated diseases in organs** *Oncotarget* **9**:7204–7218

16. Medzhitov R. (2008) **Origin and physiological roles of inflammation** *Nature* **454**:428–435

17. Medzhitov R. (2021) **The spectrum of inflammatory responses** *Science* **374**:1070–1075

18. Gerhardt T., Ley K. (2015) **Monocyte trafficking across the vessel wall** *Cardiovasc Res* **107**:321–330

19. Shi C., Pamer E.G. (2011) **Monocyte recruitment during infection and inflammation** *Nat Rev Immunol* **11**:762–774

20. Ballabio A., Bonifacino J.S. (2020) **Lysosomes as dynamic regulators of cell and organismal homeostasis** *Nat Rev Mol Cell Biol* **21**:101–118

21. Saftig P., Puertollano R. (2021) **How Lysosomes Sense, Integrate, and Cope with Stress** *Trends Biochem Sci* **46**:97–112

22. Gordon S. (2016) **Phagocytosis: An Immunobiologic Process** *Immunity* **44**:463–475

23. Kourtzelis I., Hajishengallis G., Chavakis T. (2020) **Phagocytosis of Apoptotic Cells in Resolution of Inflammation** *Front Immunol* **11**

24. Gupta S., et al. (2007) **Binding of ras to phosphoinositide 3-kinase p110alpha is required for ras-driven tumorigenesis in mice** *Cell* **129**:957–968

25. Zhao J.J., et al. (2006) **The p110alpha isoform of PI3K is essential for proper growth factor signaling and oncogenic transformation** *Proc Natl Acad Sci U S A* **103**:16296–16300

26. Zhao H., et al. (2021) **Inflammation and tumor progression: signaling pathways and targeted intervention** *Signal Transduct Target Ther* **6**

27. Biswas S.K., Mantovani A. (2010) **Macrophage plasticity and interaction with lymphocyte subsets: cancer as a paradigm** *Nat Immunol* **11**:889–896

28. Mercalli A., et al. (2013) **Rapamycin unbalances the polarization of human macrophages to M1** *Immunology* **140**:179–190

29. Paulsen O., et al. (2017) **The relationship between pro-inflammatory cytokines and pain, appetite and fatigue in patients with advanced cancer** *PLoS One* **12**

30. Swirski F.K., et al. (2009) **Identification of splenic reservoir monocytes and their deployment to inflammatory sites** *Science* **325**:612–616

31. Akashi K., Traver D., Miyamoto T., Weissman I.L. (2000) **A clonogenic common myeloid progenitor that gives rise to all myeloid lineages** *Nature* **404**:193–197

32. Tsuyada A., et al. (2012) **CCL2 mediates cross-talk between cancer cells and stromal fibroblasts that regulates breast cancer stem cells** *Cancer Res* **72**:2768–2779

33. Matsushima K., Larsen C.G., DuBois G.C., Oppenheim J.J. (1989) **Purification and characterization of a novel monocyte chemotactic and activating factor produced by a human myelomonocytic cell line** *J Exp Med* **169**:1485–1490

34. Orecchioni M., Ghosheh Y., Pramod A.B., Ley K. (2019) **Macrophage Polarization: Different Gene Signatures in M1(LPS+) vs. Classically and M2(LPS-) vs. Alternatively Activated Macrophages** *Front Immunol* **10**

35. Cui K., Ardell C.L., Podolnikova N.P., Yakubenko V.P. (2018) **Distinct Migratory Properties of M1, M2, and Resident Macrophages Are Regulated by alpha(D)beta(2) and alpha(M)beta(2) Integrin-Mediated Adhesion** *Front Immunol* **9**

36. Auffray C., Sieweke M.H., Geissmann F. (2009) **Blood monocytes: development, heterogeneity, and relationship with dendritic cells** *Annu Rev Immunol* **27**:669–692

37. Geissmann F., et al. (2010) **Development of monocytes, macrophages, and dendritic cells** *Science* **327**:656–661

38. Soler A., et al. (2013) **Inhibition of the p110alpha isoform of PI 3-kinase stimulates nonfunctional tumor angiogenesis** *J Exp Med* **210**:1937–1945

39. Faust N., Varas F., Kelly L.M., Heck S., Graf T. (2000) **Insertion of enhanced green fluorescent protein into the lysozyme gene creates mice with green fluorescent granulocytes and macrophages** *Blood* **96**:719–726

40. Schwartz A.B., et al. (2021) **Elucidating the Biomechanics of Leukocyte Transendothelial Migration by Quantitative Imaging** *Front Cell Dev Biol* **9**

41. Vicente-Manzanares M., Sanchez-Madrid F. (2004) **Role of the cytoskeleton during leukocyte responses** *Nat Rev Immunol* **4**:110–122

42. McWhorter F.Y., Wang T., Nguyen P., Chung T., Liu W.F. (2013) **Modulation of macrophage phenotype by cell shape** *Proc Natl Acad Sci U S A* **110**:17253–17258

43. Pollard T.D., Cooper J.A. (2009) **Actin, a central player in cell shape and movement** *Science* **326**:1208–1212

44. Ronzier E., et al. (2022) **The Actin Cytoskeleton Responds to Inflammatory Cues and Alters Macrophage Activation** *Cells* **11**

45. Hajishengallis G., Lambris J.D. (2016) **More than complementing Tolls: complement-Toll-like receptor synergy and crosstalk in innate immunity and inflammation** *Immunol Rev* **274**:233–244

46. Reis E.S., Mastellos D.C., Hajishengallis G., Lambris J.D. (2019) **New insights into the immune functions of complement** *Nat Rev Immunol* **19**:503–516

47. Underhill D.M., Goodridge H.S. (2012) **Information processing during phagocytosis** *Nat Rev Immunol* **12**:492–502

48. Yadati T., Houben T., Bitorina A., Shiri-Sverdlov R. (2020) **The Ins and Outs of Cathepsins: Physiological Function and Role in Disease Management** *Cells* **9**

49. Shinoda H., Shannon M., Nagai T. (2018) **Fluorescent Proteins for Investigating Biological Events in Acidic Environments** *Int J Mol Sci* **19**

50. Mota A.C., et al. (2021) **Lysosome-Dependent LXR and PPARdelta Activation Upon Efferocytosis in Human Macrophages** *Front Immunol* **12**

51. Qiu H., et al. (2023) **Efferocytosis: An accomplice of cancer immune escape** *Biomed Pharmacother* **167**

52. Fredman G., Li Y., Dalli J., Chiang N., Serhan C.N. (2012) **Self-limited versus delayed resolution of acute inflammation: temporal regulation of pro-resolving mediators and microRNA** *Sci Rep* **2**

53. Meizlish M.L., Franklin R.A., Zhou X., Medzhitov R. (2021) **Tissue Homeostasis and Inflammation** *Annu Rev Immunol* **39**:557–581

54. Wilson K., et al. (2013) **Mechanisms of leading edge protrusion in interstitial migration** *Nat Commun* **4**

55. Soriano O., Alcon-Perez M., Vicente-Manzanares M., Castellano E. (2021) **The Crossroads between RAS and RHO Signaling Pathways in Cellular Transformation, Motility and Contraction** *Genes (Basel)* **12**

56. Hoon J.L., Tan M.H., Koh C.G. (2016) **The Regulation of Cellular Responses to Mechanical Cues by Rho GTPases** *Cells* **5**

57. Wolfenson H., Yang B., Sheetz M.P. (2019) **Steps in Mechanotransduction Pathways that Control Cell Morphology** *Annu Rev Physiol* **81**:585–605

58. Kamnev A., Lacouture C., Fusaro M., Dupre L. (2021) **Molecular Tuning of Actin Dynamics in Leukocyte Migration as Revealed by Immune-Related Actinopathies** *Front Immunol* **12**

59. Scerra G., et al. (2022) **Lysosomal positioning diseases: beyond substrate storage** *Open Biol* **12**

60. Ferreira C.R., Gahl W.A. (2017) **Lysosomal storage diseases** *Transl Sci Rare Dis* **2**:1–71

61. Liu T., Zhang L., Joo D., Sun S.C. (2017) **NF-kappaB signaling in inflammation** *Signal Transduct Target Ther* **2**

62. Tak P.P., Firestein G.S. (2001) **NF-kappaB: a key role in inflammatory diseases** *J Clin Invest* **107**:7–11

63. de Mingo A., et al. (2016) **Cysteine cathepsins control hepatic NF-kappaB-dependent inflammation via sirtuin-1 regulation** *Cell Death Dis* **7**

64. Yang N., Wang P., Wang W.J., Song Y.Z., Liang Z.Q. (2015) **Inhibition of cathepsin L sensitizes human glioma cells to ionizing radiation in vitro through NF-kappaB signaling pathway** *Acta Pharmacol Sin* **36**:400–410

65. Chang C.P., Su Y.C., Hu C.W., Lei H.Y. (2013) **TLR2-dependent selective autophagy regulates NF-kappaB lysosomal degradation in hepatoma-derived M2 macrophage differentiation** *Cell Death Differ* **20**:515–523

66. Liu N., et al. (2003) **NF-kappaB protects from the lysosomal pathway of cell death** *EMBO J* **22**:5313–5322

67. Kast D.J., Dominguez R. (2017) **The Cytoskeleton-Autophagy Connection** *Curr Biol* **27**:R318–R326

68. Taunton J., et al. (2000) **Actin-dependent propulsion of endosomes and lysosomes by recruitment of N-WASP** *J Cell Biol* **148**:519–530

69. Ettelt R.V.G., Didusch S., Riemelmoser B., Ehrenreiter K., Hartl M., Huber L.A., Baccarini M. (2023) **Interplay between PLEKHG3-regulated actin dynamics and lysosomal trafficking in cell motility** *BioRxiv*

70. Stockinger W., et al. (2006) **Differential requirements for actin polymerization, calmodulin, and Ca2+ define distinct stages of lysosome/phagosome targeting** *Mol Biol Cell* **17**:1697–1710

71. Hryciw D.H., Lee E.M., Pollock C.A., Poronnik P. (2004) **Molecular changes in proximal tubule function in diabetes mellitus** *Clin Exp Pharmacol Physiol* **31**:372–379

72. Gong G.Q., et al. (2023) **A small-molecule PI3Kalpha activator for cardioprotection and neuroregeneration** *Nature* **618**:159–168

73. Jorba I., Uriarte J.J., Campillo N., Farre R., Navajas D. (2017) **Probing Micromechanical Properties of the Extracellular Matrix of Soft Tissues by Atomic Force Microscopy** *J Cell Physiol* **232**:19–26

74. Rico F., et al. (2005) **Probing mechanical properties of living cells by atomic force microscopy with blunted pyramidal cantilever tips** *Phys Rev E Stat Nonlin Soft Matter Phys* **72**

75. McCarthy D.J., Chen Y., Smyth G.K. (2012) **Differential expression analysis of multifactor RNA-Seq experiments with respect to biological variation** *Nucleic Acids Res* **40**:4288–4297

76. Robinson M.D., McCarthy D.J., Smyth G.K. (2010) **edgeR: a Bioconductor package for differential expression analysis of digital gene expression data** *Bioinformatics* **26**:139–140

77. Campos-Laborie F.J., et al. (2019) **DECO: decompose heterogeneous population cohorts for patient stratification and discovery of sample biomarkers using omic data profiling** *Bioinformatics* **35**:3651–3662

78. Killcoyne S., Carter G.W., Smith J., Boyle J. (2009) **Cytoscape: a community-based framework for network modeling** *Methods Mol Biol* **563**:219–239

79. Franz M., et al. (2018) **GeneMANIA update 2018** *Nucleic Acids Res* **46**:W60–W64

Author information

Alejandro Rosell[#]

Tumour-Stroma Signalling Lab., Centro de Investigación del Cáncer, Instituto de Biología Molecular y Celular del Cáncer, Consejo Superior de Investigaciones Científicas (CSIC)-Universidad de Salamanca, Campus Miguel de Unamuno, Salamanca, Spain

[#]These authors contributed equally to this work

Agata A Krygowska[#]

Centre for Cancer and Inflammation, Barts Cancer Institute, Queen Mary University of London, London, United Kingdom

[#]These authors contributed equally to this work

Marta Alcón Pérez
Tumour-Stroma Signalling Lab., Centro de Investigación del Cáncer, Instituto de Biología Molecular y Celular del Cáncer, Consejo Superior de Investigaciones Científicas (CSIC)-Universidad de Salamanca, Campus Miguel de Unamuno, Salamanca, Spain

Cristina Cuesta
Tumour-Stroma Signalling Lab., Centro de Investigación del Cáncer, Instituto de Biología Molecular y Celular del Cáncer, Consejo Superior de Investigaciones Científicas (CSIC)-Universidad de Salamanca, Campus Miguel de Unamuno, Salamanca, Spain

Mathieu-Benoit Voisin
Centre for Microvascular Research, William Harvey Research Institute, Queen Mary University of London, London, United Kingdom

Juan de Paz
Tumour-Stroma Signalling Lab., Centro de Investigación del Cáncer, Instituto de Biología Molecular y Celular del Cáncer, Consejo Superior de Investigaciones Científicas (CSIC)-Universidad de Salamanca, Campus Miguel de Unamuno, Salamanca, Spain

Héctor Sanz-Fraile
Unit of Biophysics and Bioengineering, Department of Biomedicine, School of Medicine and Health Sciences, Universitat de Barcelona, Barcelona, Spain

Vinothini Rajeeve
Centre for Cancer Genomics and Computational Biology, Cell Signalling and Proteomics Laboratory, Barts Cancer Institute, Queen Mary University of London, London, United Kingdom
ORCID iD: 0000-0002-6361-4291

Alberto Berral-González
Bioinformatics and Functional Genomics, Centro de Investigación del Cáncer, Instituto de Biología Molecular y Celular del Cáncer, Consejo Superior de Investigaciones Científicas (CSIC)-Universidad de Salamanca, Campus Miguel de Unamuno, Salamanca, Spain

Ana Carreras-González
Inflammation and Macrophage Plasticity Lab, CIC bioGUNE, Derio, Spain

Ottilie Swinyard
Centre for Cancer and Inflammation, Barts Cancer Institute, Queen Mary University of London, London, United Kingdom

Enrique Gabandé-Rodriguez
Centre for Cancer and Inflammation, Barts Cancer Institute, Queen Mary University of London, London, United Kingdom
ORCID iD: 0000-0002-9715-8714

Julian Downward
Oncogene Biology Laboratory, Francis Crick Institute, London, United Kingdom
ORCID iD: 0000-0002-2331-4729

Jordi Alcaraz
Unit of Biophysics and Bioengineering, Department of Biomedicine, School of Medicine and Health Sciences, Universitat de Barcelona, Barcelona, Spain, Institute for Bioengineering of Catalonia (IBEC), The Barcelona Institute for Science and Technology (BIST), Barcelona, Spain

Juan Anguita
Inflammation and Macrophage Plasticity Lab, CIC bioGUNE, Derio, Spain, Ikerbasque, Basque Foundation for Science, Bilbao, Spain

Carmen García-Macías
Pathology Unit, Centro de Investigación del Cáncer, Instituto de Biología Molecular y Celular del Cáncer, Universidad de Salamanca, Campus Miguel de Unamuno, Salamanca, Spain

Javier De Las Rivas
Bioinformatics and Functional Genomics, Centro de Investigación del Cáncer, Instituto de Biología Molecular y Celular del Cáncer, Consejo Superior de Investigaciones Científicas (CSIC)-Universidad de Salamanca, Campus Miguel de Unamuno, Salamanca, Spain

Pedro Cutillas
Centre for Cancer Genomics and Computational Biology, Cell Signalling and Proteomics Laboratory, Barts Cancer Institute, Queen Mary University of London, London, United Kingdom
ORCID iD: 0000-0002-3426-2274

Esther Castellano
Tumour-Stroma Signalling Lab., Centro de Investigación del Cáncer, Instituto de Biología Molecular y Celular del Cáncer, Consejo Superior de Investigaciones Científicas (CSIC)-Universidad de Salamanca, Campus Miguel de Unamuno, Salamanca, Spain, Centre for Cancer and Inflammation, Barts Cancer Institute, Queen Mary University of London, London, United Kingdom
ORCID iD: 0000-0002-8449-4081

For correspondence: ecastellano@usal.es

Editors

Reviewing Editor
Florent Ginhoux
Singapore Immunology Network, Singapore, Singapore

Senior Editor
Tadatsugu Taniguchi
University of Tokyo, Tokyo, Japan

Reviewer #1 (Public review):

This study by Alejandro Rosell et al. reveals the immunoregulatory role of the RAS-p110α pathway in macrophages, specifically in regulating monocyte extravasation and lysosomal digestion during inflammation. Disrupting this pathway, through genetic tools or pharmacological intervention in mice, impairs the inflammatory response, leading to delayed resolution and more severe acute inflammation. The authors suggest that activating p110α with small molecules could be a potential therapeutic strategy for treating chronic

inflammation. These findings provide important insights into the mechanisms by which p110α regulates macrophage function and the overall inflammatory response.

The updates made by the authors in the revised version have addressed the main points raised in the initial review, further improving the strength of their findings.

https://doi.org/10.7554/eLife.94590.2.sa2

Reviewer #2 (Public review):

Summary:

Cell intrinsic signaling pathways controlling the function of macrophages in inflammatory processes, including in response to infection, injury or in the resolution of inflammation are incompletely understood. In this study, Rosell et al. investigate the contribution of RAS-p110α signaling to macrophage activity. p110α is a ubiquitously expressed catalytic subunit of PI3K with previously described roles in multiple biological processes including in epithelial cell growth and survival, and carcinogenesis. While previous studies have already suggested a role for RAS-p110α signaling in macrophage function, the cell intrinsic impact of disrupting the interaction between RAS and p110α in this central myeloid cell subset is not known.

Strengths:

Exploiting a sound previously described genetically engineered mouse model that allows tamoxifen-inducible disruption of the RAS-p110α pathway and using different readouts of macrophage activity in vitro and in vivo, the authors provide data consistent with their conclusion that alteration in RAS-p110α signaling impairs various but selective aspects of macrophage function in a cell-intrinsic manner.

Weaknesses:

My main concern is that for various readouts, the difference between wild-type and mutant macrophages in vitro or between wild-type and Pik3caRBD mice in vivo is modest, even if statistically significant. To further substantiate the extent of macrophage function alteration upon disruption of RAS-p110α signaling and its impact on the initiation and resolution of inflammatory responses, the manuscript would benefit from a more extensive assessment of macrophage activity and inflammatory responses in vivo.

In the in vivo model, all cells have disrupted RAS-p100α signaling, not only macrophages. Given that other myeloid cells besides macrophages contribute to the orchestration of inflammatory responses, it remains unclear whether the phenotype described in vivo results from impaired RAS-p100α signaling within macrophages or from defects in other haematopoietic cells such as neutrophils, dendritic cells, etc.

Inclusion of information on the absolute number of macrophages, and total immune cells (e.g. for the spleen analysis) would help determine if the reduced frequency of macrophages represents an actual difference in their total number or rather reflects a relative decrease due to an increase in the number of other/s immune cell/s.

https://doi.org/10.7554/eLife.94590.2.sa1

Author response:

The following is the authors' response to the original reviews.

Public Reviews:

Reviewer #1 (Public Review):

In this study, Alejandro Rosell et al. uncovers the immunoregulation functions of RAS-p110α pathway in macrophages, including the extravasation of monocytes from the bloodstream and subsequent lysosomal digestion. Disrupting RAS-p110α pathway by mouse genetic tools or by pharmacological intervention, hampers the inflammatory response, leading to delayed resolution and more severe acute inflammatory reactions. The authors proposed that activating p110α using small molecules could be a promising approach for treating chronic inflammation. This study provides insights into the roles and mechanisms of p110α on macrophage function and the inflammatory response, while some conclusions are still questionable because of several issues described below.

(1) Fig. 1B showed that disruption of RAS-p110α causes the decrease in the activation of NF-κB, which is a crucial transcription factor that regulates the expression of proinflammatory genes. However, the authors observed that disruption of RAS-p110α interaction results in an exacerbated inflammatory state in vivo, in both localized paw inflammation and systemic inflammatory mediator levels. Also, the authors introduced that "this disruption leads to a change in macrophage polarization, favoring a more proinflammatory M1 state" in introduction according to reference 12. The conclusions drew from the signaling and the models seemed contradictory and puzzling. Besides, it is not clear why the protein level of p65 was decreased at 10' and 30'. Was it attributed to the degradation of p65 or experimental variation?

We thank the reviewer for this insightful comment and apologize for not previously explaining the implications of the observed decrease in NF-κB activation. We found a decrease in NF-κB activation in response to LPS + IFN-γ stimulation in macrophages lacking RAS-PI3K interaction. As the reviewer pointed out, NF-κB is a key transcription factor that regulates the expression of various proinflammatory genes. To better characterize whether the decrease in p-p65 would lead to a reduction in the expression of specific cytokines, we performed a cytokine array using unstimulated and LPS + IFN-γ stimulated macrophages. The results indicated a small number of cytokines with altered expression, validating that RAS-p110α activation of p-p65 regulates the expression of some inflammatory cytokines. These results have been added to the manuscript and to Figure 1 (panels C and D). In brief, the data suggest an impairment in recruitment factors and inflammatory regulators following the disruption of RAS-p110α signaling in macrophages, which aligns with the observed in vivo phenotype.

Our findings indicate that the disruption of RAS-p110α signaling has a complex and multifaceted role in BMDMs. Specifically, monocytes lacking RAS-PI3K are unable to reach the inflamed area due to an impaired ability to extravasate, caused by altered actin cytoskeleton dynamics. Consequently, inflammation is sustained over time, continuously releasing inflammatory mediators. Moreover, we have shown that macrophages deficient in RAS-p110α interaction fail to mount a full inflammatory response due to decreased activation of p-p65, leading to reduced production of a set of inflammatory regulators. Additionally, these macrophages are unable to effectively process phagocytosed material and activate the resolutive phase of inflammation. As a result of these defects, an exacerbated and sustained inflammatory response occurs.

Our in vivo data, showing an increase in systemic inflammatory mediators, might be a consequence of the accumulation of monocytes produced by bone marrow progenitors in response to sensed inflammatory stimuli, but unable to extravasate.

Regarding the sentence in the introduction: "this disruption leads to a change in macrophage polarization, favoring a more proinflammatory M1 state" (reference 12), this was observed in an oncogenic context, which might differ from the role of RAS-p110α in a non-oncogenic situation, as analyzed in this work. We introduced these results as an example to establish the role of RAS-p110α in macrophages, demonstrating its participation in macrophage-dependent responses. Together with our study, these findings clearly indicate that p110α signaling is critical when analyzing full immune responses. Previously, little was known about the role of this PI3K isoform in immune responses. Our data, along with those presented by Murillo et al. (ref. 12), demonstrate that p110α plays a significant role in macrophage function in both oncogenic and inflammatory contexts. Additionally, our results suggest that this role is complex and multifaceted, warranting further investigation to fully understand the complexity of p110α signaling in macrophages.

Regarding decreased levels of p65 at 10' and 30' in RBD cells we are still uncertain about the possible molecular mechanism leading to the observed decrease. No changes in p65 mRNA levels were observed after 30 minutes of LPS+IFNγ treatment as shown in Author response image 1.

Author response image 1.

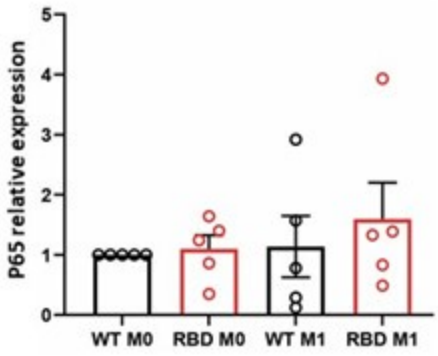

Preliminary data not shown here suggest that treating macrophages with BYL exhibits a similar effect, indicating a potential pathway for investigation. Considering that the decrease in protein levels is not due to lower mRNA expression, we may infer that post-translational mechanisms are leading to early protein degradation in RAS-p110α deficient macrophages. This could explain the observed decrease in protein activation. However, the specific molecular mechanism responsible for this degradation remains unclear, and further research is necessary to elucidate it.

> *(2) In Fig 3, the authors used bone-marrow derived macrophages (BMDMs) instead of isolated monocytes to evaluate the ability of monocyte transendothelial migration, which is not sufficiently convincing. In Fig. 3B, the authors evaluated the migration in Pik3caWT/- BMDMs, and Pik3caWT/WT BMDMs treated with BYL-719'. Given that the dose effect of gene expression, the best control is Pik3caWT/- BMDMs treated with BYL-719.*

We thank reviewer for this comment. While we agree that using BMDMs might not be the most conventional approach for studying monocyte migration, there were several reasons why we still considered them a valid method. While isolated monocytes are the initial cell type involved in transendothelial migration, bone marrow-derived macrophages (BMDMs) provide a relevant and practical model for studying this process. BMDMs are differentiated from the same bone marrow precursors as monocytes and retain the ability to respond to

chemotactic signals, adhere to endothelial cells, and migrate through the endothelium. This makes them a suitable tool for examining the cellular and molecular mechanisms underlying monocyte migration and subsequent macrophage infiltration into tissues. Additionally, BMDMs offer experimental consistency and are easier to manipulate in vitro, enabling more controlled and reproducible studies.

In response to the comment regarding Fig. 3B, we appreciate the suggestion to use Pik3ca WT/- BMDMs treated with BYL-719 as a control. However, our rationale for using Pik3ca WT/WT BMDMs treated with BYL-719 was based on a conceptual approach rather than a purely experimental control. The BYL-719 treatment in Pik3ca WT/WT cells was intended to simulate the inhibition of p110α in a fully functional, wild-type context. This allows us to directly assess the impact of p110α inhibition under normal physiological conditions, which is more representative of what would occur in an organism where the full dose of Pik3ca is present. Using Pik3ca WT/- BMDMs treated with BYL-719 as a control may not accurately reflect the in vivo scenario, where any therapeutic intervention would likely occur in the context of a fully functional, wild-type background. Our approach aims to provide a clearer understanding of how p110α inhibition affects cell functionality in a wild-type setting, which is relevant for potential therapeutic applications. Therefore, we considered the use of Pik3ca WT/WT BMDMs with BYL-719 treatment to be a more appropriate control for testing the effects of p110α inhibition in normal conditions.

> *(3) In Fig. 4E-4G, the authors observed that elevated levels of serine 3 phosphorylated Cofilin in Pik3caRBD/- BMDMs both in unstimulated and in proinflammatory conditions, and phosphorylation of Cofilin at Ser3 increase actin stabilization, it is not clear why disruption of RAS-p110α binding caused a decrease in the F-actin pool in unstimulated BMDMs?*

We thank the reviewer for this insightful comment. During the review process, we have carefully quantified all the Western blots conducted. While we did observe an increase in phospho-Cofilin (Ser3) levels in RBD BMDMs, this increase did not reach statistical significance. As a result, we cannot confidently attribute the observed increase in F-actin to this proposed mechanism. We apologize for any confusion this may have caused. Consequently, we have removed these data from Figure 4G and the associated discussion.

Unfortunately, we have not yet identified the underlying mechanism responsible for this phenotype. Future experiments will focus on exploring potential alterations in other actin-nucleating, regulating, and stabilizing proteins that could account for the observed changes in F-actin levels.

> ***Reviewer #2 (Public Review):***
>
> *Summary:*
>
> *Cell intrinsic signaling pathways controlling the function of macrophages in inflammatory processes, including in response to infection, injury or in the resolution of inflammation are incompletely understood. In this study, Rosell et al. investigate the contribution of RAS-p110α signaling to macrophage activity. p110α is a ubiquitously expressed catalytic subunit of PI3K with previously described roles in multiple biological processes including in epithelial cell growth and survival, and carcinogenesis. While previous studies have already suggested a role for RAS-p110α signaling in macrophages function, the cell intrinsic impact of disrupting the interaction between RAS and p110α in this central myeloid cell subset is not known.*
>
> *Strengths:*

> *Exploiting a sound previously described genetically mouse model that allows tamoxifen-inducible disruption of the RAS-p110α pathway and using different readouts of macrophage activity in vitro and in vivo, the authors provide data consistent with their conclusion that alteration in RAS-p110α signaling impairs the function of macrophages in a cell intrinsic manner. The study is well designed, clearly written with overall high-quality figures.*
>
> *Weaknesses:*
>
> *My main concern is that for many of the readouts, the difference between wild-type and mutant macrophages in vitro or between wild-type and Pik3caRBD mice in vivo is rather modest, even if statistically significant (e.g. Figure 1A, 1C, 2A, 2F, 3B, 4B, 4C). In other cases, such as for the analysis of the H&E images (Figure 1D-E, S1E), the images are not quantified, and it is hard to appreciate what the phenotype in samples from Pik3caRBD mice is or whether this is consistently observed across different animals. Also, the authors claim there is a 'notable decrease' in Akt activation but 'no discernible chance' in ERK activation based on the western blot data presented in Figure 1A. I do not think the data shown supports this conclusion.*

We appreciate the reviewer's careful examination of our data and their observation regarding the modest differences between wild-type and mutant macrophages in vitro, as well as between wild-type and Pik3caRBD mice in vivo. While the differences observed in Figures 1A, 1C, 2A, 2F, 3B, 4B, and 4C are statistically significant but modest, our data demonstrate that they are biologically relevant and should be interpreted within the specific nature of our model. Our study focuses on the disruption of the RASp110α interaction, but it should be noted that alternative pathways for p110α activation, independent of RAS, remain functional in this model. Additionally, the model retains the expression of other p110 isoforms, such as p110β, p110γ, and p110δ, which are known to have significant roles in immune responses. Given the overlapping functions of these p110 isoforms, and the fact that our model involves a subtle modification that specifically affects the RAS-p110α interaction without completely abrogating p110α activity, it is understandable that only modest effects are observed in some readouts. The redundancy and compensation by other p110 isoforms likely mitigate the impact of disrupting RAS-mediated p110α activation.

However, despite these modest in vitro differences, it is crucial to highlight that the in vivo effects on inflammation are both clear and consistent. The persistence of inflammation in our model suggests that the RAS-p110α interaction plays a specific, non-redundant role in resolving inflammation, which cannot be fully compensated by other signaling pathways or p110 isoforms. These findings underscore the importance of RAS-p110α signaling in immune homeostasis and suggest that even subtle disruptions in this pathway can lead to significant physiological consequences over time, particularly in the context of inflammation. The modest differences observed may represent early or subtle alterations that could lead to more pronounced phenotypes under specific stress or stimulation conditions. This could be tested across all the figures mentioned. For instance, in Fig. 1A, the Western blot for AKT has been quantified, demonstrating a significant decrease in AKT levels; in Fig. 1C, although the difference in paw inflammation was only a few millimeters in thickness, considering the size of a mouse paw, those millimeters were very noticeable by eye. Furthermore, pathological examination of the tissue consistently showed an increase in inflammation in RBD mice. Furthermore, the consistency of the observed differences across different readouts and experimental setups reinforces the reliability and robustness of our findings. Even modest changes that are consistently observed across different assays and conditions are indicative of genuine biological effects. The statistical significance of the differences indicates that they are unlikely to be due to random variation. This statistical rigor supports the conclusion that the observed effects, albeit modest, are real and warrant further exploration.

Regarding the analysis of H&E images, we have now quantified the changes with the assistance of the pathologist, Mª Carmen García Macías, who has been added to the author list. We removed the colored arrows from the images and instead quantified fibrin and chromatin remnants as markers of inflammation staging. Loose chromatin, which increases as a consequence of cell death, is higher in the early phases of inflammation and decreases as macrophages phagocytose cell debris to initiate tissue healing. Chromatin content was scored on a scale from 1 to 3, where 1 represents the lowest amount and 3 the highest. The scoring was based on the area within the acute inflammatory abscess where chromatin could be found: 3 for less than 30%, 2 for 30-60%, and 1 for over 60%. Graphs corresponding to this quantification have now been added to Figure 1 and an explanation of the scale has been added to Material and Methods.

> *To further substantiate the extent of macrophage function alteration upon disruption of RAS-p110α signaling, the manuscript would benefit from testing macrophage activity in vitro and in vivo across other key macrophage activities such as bacteria phagocytosis, cytokine/chemokine production in response to titrating amounts of different PAMPs, inflammasome function, etc. This would be generally important overall but also useful to determine whether the defects in monocyte motility or macrophage lysosomal function are selectively controlled downstream of RAS-p110α signaling.*

We thank reviewer #2 for this comment. In order to better address the role of RAS-PI3K in macrophage function, we have performed some additional experiments, some of which have been added to the revised version of the manuscript.

(1) We have performed cytokine microarrays of RAS-p110α deficient macrophages unstimulated and stimulated with LPS+IFN-g. Results have been added to the manuscript and to Supplementary Figure S1E and S1F. In brief, the data obtained suggest an impairment in recruitment factors, as well as in inflammatory regulators after disruption of RAS-p110α signaling in macrophages, which align with the in vivo observed phenotype.

(2) We also conducted phagocytosis assays to analyze the ability of RAS-p110α deficient macrophages to phagocytose 1 µm Sepharose beads, *Borrelia burgdorferi*, and apoptotic cells. The data reveal varied behavior of RAS-p110α deficient bone marrow-derived macrophages (BMDMs) depending on the target:

• Engulfment of Non-biological Particles: RAS-p110α deficient macrophages showed a decreased ability to engulf 1 µm Sepharose beads. This suggests that RAS-p110α signaling is important for the effective phagocytosis of non-biological particles. These findings have now been added to the text and figures have been added to supplementary Fig. S4A

• Response to Bacterial Pathogens: When exposed to *Borrelia burgdorferi*, RAS-p110α deficient macrophages did not exhibit a change in bacterial uptake. This indicates that RAS-p110α may not play a critical role in the initial phagocytosis of this bacterial pathogen. The observed increase in the phagocytic index, although not statistically significant, might imply a compensatory mechanism or a more complex interaction that warrants further investigation. These findings have now been added to the text and figures have been added to supplementary Fig. S4B. These experiments were performed in collaboration with Dr. Anguita, from CICBioBune (Bilbao, Spain) and, as a consequence, he has been added as an author in the paper.

• Phagocytosis of Apoptotic Cells: There were no differences in the phagocytosis rate of apoptotic cells between RAS-p110α deficient and control macrophages at early time points. However, the accumulation of engulfed material at later time points suggests a possible delay in the processing and degradation of apoptotic cells in the absence of RAS-p110α signaling.

These findings highlight the complexity of RAS-p110α's involvement in phagocytic processes and suggest that its role may vary with different types of phagocytic targets.

> *Furthermore, given the key role of other myeloid cells besides macrophages in inflammation and immunity it remains unclear whether the phenotype observed in vivo can be attributed to impaired macrophage function. Is the function of neutrophils, dendritic cells or other key innate immune cells not affected?*

Thank you for this insightful comment. We understand the key role of other myeloid cells in inflammation and immunity. However, our study specifically focuses on the role of macrophages. Our data show that disruption of RAS-PI3K leads to a clear defect in macrophage extravasation, and our in vitro data demonstrate issues in macrophage cytoskeleton and phagocytosis, aligning with the in vivo phenotype.

Experiments investigating the role of RAS-PI3K in neutrophils, dendritic cells, or other innate immune cells are beyond the scope of this study. Understanding these interactions would indeed require separate, comprehensive studies and the generation of new mouse models to disrupt RAS-PI3K exclusively in specific cell types.

Furthermore, during paw inflammation experiments, polymorphonuclear cells were present from the initial phases of the inflammatory response. What caught our attention was the prolonged presence of these cells. In conversation with our in-house pathologist, she mentioned the lack of macrophages to remove dead polymorphonuclear cells in our RAS-PI3K mutant mice. Specific staining for macrophages confirmed the absence of macrophages in the inflamed node of mutant mice.

We acknowledge that further research is necessary to elucidate the effects on other myeloid cells. However, our current findings provide clear evidence of a decrease in inflammatory monocytes and defective macrophage responses to inflammation, both in vivo and in vitro. We believe these results significantly contribute to understanding the role of RAS-PI3K in macrophage function during inflammation.

> *Compelling proof of concept data that targeting RAS-p110α signalling constitutes indeed a putative approach for modulation of chronic inflammation is lacking. Addressing this further would increase the conceptual advance of the manuscript and provide extra support to the authors' suggestion that p110α inhibition or activation constitute promising approaches to manage inflammation.*

We thank Reviewer #2 for this insightful comment. In our manuscript, we have demonstrated through multiple experiments that the inhibition of p110α, either by disrupting RAS-p110α signaling or through the use of Alpelisib (BYL-719), has a modulatory effect on inflammatory responses. However, we acknowledge that we have not activated the pathway due to the unavailability of a suitable p110α activator until the concluding phase of our study.

We recognize the importance of this point and are eager about investigating both the inhibition and activation of p110α as potential approaches to managing inflammation in well-established inflammatory disease models. We believe that such comprehensive studies would significantly enhance the conceptual advance and translational relevance of our findings.

However, it is essential to note that the primary aim of our current work was to demonstrate the role of RAS-p110α in the inflammatory responses of macrophages. We have successfully shown that RASp110α influences macrophage behavior and inflammatory signaling. Expanding the scope to include disease models and pathway activation studies would be an extensive project that goes beyond the current objectives of this manuscript. While our present study establishes the foundational role of RASp110α in macrophage-mediated

inflammatory responses, we agree that further investigation into both p110α inhibition and activation in disease models is crucial. We are keen to pursue this line of research in future studies, which we believe will provide robust evidence supporting the therapeutic potential of targeting RAS-p110α signaling in chronic inflammation.

> *Finally, the analysis by FACS should also include information about the total number of cells, not just the percentage, which is affected by the relative change in other populations. On this point, Figure S2B shows a substantial, albeit not significant (with less number of mice analysed), increase in the percentage of CD3+ cells. Is there an increase in the absolute number of T cells or does this apparent relative increase reflect a reduction in myeloid cells?*

We thank the reviewer for this comment, which we have addressed in the revised version of the manuscript. Regarding the total number of cells analyzed, we have added to the Materials and Methods section that in all our studies, a total of 50,000 cells were analyzed (line 749). The percentages of cells are related to these 50,000 events. Additionally, we have increased the number of mice analyzed by including new mice for CD3+ cell analysis. Despite this, the results remain not significant.

> ***Recommendations for the authors:***
>
> ***Reviewer #1 (Recommendations For The Authors):***
>
> *(1) It is recommended to provide a graphical abstract to summarize the multiple functions of RAS-p110α pathway in monocyte/macrophages that the authors proposed*

We thank reviewer for this useful recommendation. A graphical abstract has now been added to the study.

> *(2) Western blots in this paper need quantification and a measure of reproducibility*

We have now added a graph with the quantification of the western blots performed in this work as a measure of reproducibility.

> *(3) Representative flow data and gating strategy should be included*

We have now added the description of the gating strategy followed to material and methods section.

https://doi.org/10.7554/eLife.94590.2.sa0